Online correction of drift in structural identification using artificial white noise observations and an unscented Kalman Filter

Eleni N. Chatzi[*1] and Clemente Fuggini[2a]

[1]*Institute of Structural Engineering, ETH Zurich, Wolfgang-Pauli-Strasse 15, CH-8093, Switzerland*
[2]*Industrial Innovation Division, D'Appolonia S.p.A., Via San Nazaro 19, 16145 Genova, Italy*

Abstract. In recent years the monitoring of structural behavior through acquisition of vibrational data has become common practice. In addition, recent advances in sensor development have made the collection of diverse dynamic information feasible. Other than the commonly collected acceleration information, Global Position System (GPS) receivers and non-contact, optical techniques have also allowed for the synchronous collection of highly accurate displacement data. The fusion of this heterogeneous information is crucial for the successful monitoring and control of structural systems especially when aiming at real-time estimation. This task is not a straightforward one as measurements are inevitably corrupted with some percentage of noise, often leading to imprecise estimation. Quite commonly, the presence of noise in acceleration signals results in drifting estimates of displacement states, as a result of numerical integration. In this study, a new approach based on a time domain identification method, namely the Unscented Kalman Filter (UKF), is proposed for correcting the "drift effect" in displacement or rotation estimates in an online manner, i.e., on the fly as data is attained. The method relies on the introduction of artificial white noise (WN) observations into the filter equations, which is shown to achieve an online correction of the drift issue, thus yielding highly accurate motion data. The proposed approach is demonstrated for two cases; firstly, the illustrative example of a single degree of freedom linear oscillator is examined, where availability of acceleration measurements is exclusively assumed. Secondly, a field inspired implementation is presented for the torsional identification of a tall tower structure, where acceleration measurements are obtained at a high sampling rate and non-collocated GPS displacement measurements are assumed available at a lower sampling rate. A multi-rate Kalman Filter is incorporated into the analysis in order to successfully fuse data sampled at different rates.

1. Introduction

In the past two decades, Structural Health Monitoring (SHM) using vibration measurements has attracted considerable attention in various engineering fields, including the aerospace (Basseville *et al.* 2007), (Bucharles and Vacher 2002); mechanical (Mani *et al.* 2006), (Doebling *et*

∗Corresponding author, Assistant Professor, E-mail: chatzi@ibk.baug.ethz.ch
[a] Ph.D., E-mail: clemente.fuggini@dappolonia.it

al. 2009); and civil engineering (Yuen and Katafygiotis 2006), (Papadimitriou *et al*. 2011), (Moaveni *et al*. 2011), (Fraraccio *et al*. 2008) communities. In order to conduct online monitoring, real-time control, and system identification of structural parameters, the availability of acceleration response measurements as well as displacement response data is often required. Recent years have delivered tremendous advances in sensor technologies for dynamic system monitoring, including wireless applications (Gao *et al*. 2006); highly accurate MEMS sensors; laser technologies; interferometric radar techniques; and global positioning system (GPS) receivers. This, in turn, allowed the acquisition of highly accurate acceleration, velocity and position records at high sampling rates (Psimoulis and Stiros 2008). In the presence of advanced hardware solutions at a relatively low cost, spatially dense heterogeneous sensor arrays have now become feasible solutions for the monitoring of large-scale civil structures.

In any Structural Health Monitoring (SHM) scheme applied to a civil structure, accuracy, durability and availability are requirements that must be strictly satisfied in order to guarantee reliable long-term applications. For maximizing the information and increasing the quality of data obtained through sensors, data processing techniques relying on fusion have come forth. Such techniques utilize underlying mathematical models or simple physical principles in order to extract improved information from recorded signals. Acceleration information in particular is more readily available at high sampling rates and independent of a fixed-reference point. Therefore it is often used for extraction of integral quantities such as velocity or displacement (Berg and Housner 1961, Boore and Bommer 2005). However, information extracted through acceleration is often related to shortcomings such as a random phase error, as indicated in the work of Moschas and Stiros (Moschas and Stiros 2012), or more commonly, to inaccurate, drifting estimates of integral quantities, such as displacement (Stiros 2008).

The "drift effect" is a result of the numerical integration of the low frequency noise contained in the data. Naturally, integration errors are even more pronounced in the presence of fluctuations in the sampling rate which might occur depending on the accuracy of the available data acquisition unit (Stiros and Kokkinou 2008). This effect is detrimental for implementations in structural control or early warning systems, which largely rely on the detection of extreme levels of displacement or force. Within the context of force and state tracking, state-of-the-art identification approaches dealing with the joint input-response identification problem (Naets *et al.* 2013), (Lourens *et al.* 2012) are highly effected by such biases. Throughout the literature, various methods are found for tackling this reoccurring issue. Most commonly, acceleration data is filtered with some high pass filter, thus removing low frequency content, and subsequently integrated or detrended. The major drawback of such an approach, is that it obviously leads to a process that is no longer enforced in real-time, as the post processing of windowed data is obligatory. Additionally, as will be shown in the application sections, this process is in fact a highly invasive one, often leading to erroneous signal estimates for the integral quantities, i.e., displacement or rotation.

In a more effective data processing approach, the aforementioned availability of various types of information can be exploited in order to improve data quality through fusion (Park *et al* 2013). Several works have pointed out the benefit of fusing acceleration and displacement response data for obtaining improved real-time estimates through appropriate Kalman filtering techniques (Chatzi and Smyth 2009), (Smyth and Wu 2007), (Kim *et al*. 2014). As noted in the work of (Kim *et al*. 2014), displacements estimated through filtering might still suffer from drifts, especially when dealing with a large interval of displacement updates and significant acceleration measurement errors. In order to deal with this issue, smoothing techniques can be enforced for

enhancing the accuracy of the filtering formulation. Unlike the real-time implementation of Kalman filtering, fixed-interval smoothing is implemented off-line, or at best in a "near-online" manner using some portion of the time histories of the measured data. In this paper, a novel approach is presented for obtaining an improved estimate, i.e., removing the drift issue, in an online manner.

Naturally, a number of challenges arise when seeking to estimate response on the fly through noisy (Hong *et al.* 2013) or incomplete observations (Beck *et al.* 1999). A first intricacy is related to the fact that the system itself, or the observed quantities, might comprise a nonlinear function of the states. For this purpose, identification techniques suitable for handling nonlinearities are required. State-of-the-art nonlinear identification techniques include the Least Squares Estimation (LSE) (Smyth and Wu 2007), (Lin *et al.* 2001), the extended Kalman Filter (EKF) (Mariani and Corigliano 2005), the Unscented Kalman Filter (UKF) (Wan and Van Der Merwe 2000), (Chatzi and Smyth 2009) and the sequential Monte Carlo methods (particle filters, PF) (Chen *et al.* 2005), (Maskell and Gordon 2001).

The approach introduced herein, relies on one of the aforementioned time domain identification methods, namely the UKF, for correcting displacement drift in real-time. The UKF is selected as it has proven to be quite suitable for online implementation and is also quite adept in handling noise (Chatzi *et al.* 2010). The critical innovation, enabling the success of this scheme, consists in the introduction of artificial white noise (WN) observations into the filter equations, for the unobserved displacement quantities. This results in an on-line correction of the drift issue, thus yielding highly accurate motion data. The presented numerical application binds theoretical and computational tools together, demonstrating the potential in improving signal accuracy and succeeding in real-time prediction of structural response.

The presented work is organized as follows. Firstly, the workings of the linear KF and of its nonlinear equivalent (UKF) are outlined in Section 2 for reasons of completeness. Moreover, the principles of the multi-rate and Smoothing schemes are customized for implementation with the UKF. In Section 3 the workings of the proposed artificial white noise observation approach are illustrated through a simple example. In Section 4, a single degree of freedom oscillator problem of varying complexity is presented, demonstrating the efficacy of the method given acceleration information. Finally, in Section 5 the proposed approach is validated on a displacement and acceleration fusion problem, for a simulation experiment on the monitoring of a super-tall tower structure in China. Section 6 concludes the work.

2. Computational tools

Consider a linear dynamical system described by the following continuous state-space (process) equation

$$\dot{\mathbf{x}}(t) = \mathbf{A}_c \mathbf{x}(t) + \mathbf{B}_c \mathbf{u}(t) + \mathbf{w}(t) \tag{1}$$

where $\mathbf{x}(t) \in \mathfrak{R}^n$ is the state variable vector at time t, $\mathbf{A}_c$, $\mathbf{B}_c$ are the continuous state and input matrices, $\mathbf{u}(t)$ is the input force vector, and $\mathbf{w}(t)$ is the zero mean Gaussian process noise vector with covariance matrix $\mathbf{Q}(t)$.

Using numerical integration methods, such as the fourth order Runge – Kutta scheme, Eq. (1)

can be rewritten as follows in discrete time

$$\mathbf{x}_{k+1} = \mathbf{A}\mathbf{x}_k + \mathbf{B}\mathbf{u}_k + \mathbf{w}_k \tag{2}$$

where $\mathbf{x}_k, \mathbf{u}_k \in \Re^n$ are the state variable vectors at $t = k\Delta t$, $\mathbf{w}_k$ is the process noise vector with covariance matrix $\mathbf{Q}_k$, and the discrete state and input matrices $\mathbf{A}$, $\mathbf{B}$ are obtained from Eq. (1) via integration. Additionally, the linear measurement (observation) equation at time $t = k\Delta t$ is

$$\mathbf{y}_k = \mathbf{C}\mathbf{x}_k + \boldsymbol{\upsilon}_k \tag{3}$$

where $\mathbf{y}_k \in \Re^m$ is the zero mean observation vector at $t = k\Delta t$, $\mathbf{C}$ is the observation matrix, and $\boldsymbol{\upsilon}_k$ is the zero mean Gaussian measurement noise vector with corresponding covariance matrix $\mathbf{R}_k$.

2.1 The discrete Kalman Filter

The linear Kalman Filter (KF) aims at estimating the state vector $\mathbf{x}_k \in \Re^n$ of a discrete system that is governed by the linear stochastic difference Eq. (2) and the observation Eq. (3). The estimate is based on m observations of vector $\mathbf{y}_k$, $k = 1 \dots m$. An important note is that $\mathbf{y}_k$ can be composed of partial information, i.e., not all structural dofs need to be monitored (measured).

Let's define $\hat{\mathbf{x}}_{k-1} \in \Re^n$ to be an estimate of the state at time $k-1$. Then a prior estimate of the state $\hat{\mathbf{x}}_k^-$, at time k, can be obtained via the state space equation

$$\hat{\mathbf{x}}_k^- = \mathbf{A}\hat{\mathbf{x}}_{k-1} + \mathbf{B}\mathbf{u}_{k-1} + \mathbf{w}_{k-1} \tag{4}$$

A posterior state estimate is then defined as a linear combination of the prior estimate (Prediction Step) and the weighted difference between an actual measurement and a measurement prediction (Update Step) as shown below

$$\hat{\mathbf{x}}_k = \underbrace{\hat{\mathbf{x}}_k^-}_{\text{Prediction Step}} + \underbrace{\mathbf{K}(\mathbf{y}_k - \mathbf{C}\hat{\mathbf{x}}_k^-)}_{\text{Update Step}} \tag{5}$$

The difference $(\mathbf{y}_k - \mathbf{C}\hat{\mathbf{x}}_k^-)$ is termed the measurement innovation, or residual. It reflects the discrepancy between the predicted measurement $\mathbf{C}\hat{\mathbf{x}}_k^-$ and the actual measurement $\mathbf{y}_k$.

The matrix $\mathbf{K}$, known as the Kalman gain, is essentially a gain or blending factor that minimizes the posterior error covariance defined as

$$\mathbf{P}_k = E[\mathbf{e}_k \mathbf{e}_k^T] \quad \text{where,} \quad \mathbf{e}_k = \mathbf{x}_k - \hat{\mathbf{x}}_k \tag{6}$$

The goal is to minimize the expected value of the square of the magnitude of vector $\mathbf{e}_k$. This is

equivalent to minimizing the trace of the a posteriori estimate covariance matrix $\mathbf{P}_k$, which eventually leads to:

$$\mathbf{K}_k = \mathbf{P}_k \mathbf{C}^T (\mathbf{C}\mathbf{P}_k^- \mathbf{C}^T + \mathbf{R})^{-1} \tag{7}$$

Looking at the above expression, it follows that as the measurement error covariance $\mathbf{R}$ approaches zero, the gain $\mathbf{K}$ influences the residual more heavily, i.e., the actual measurement is "trusted" more. On the other hand, as the prior estimate error covariance $\mathbf{P}_k^-$ approaches zero, the gain $\mathbf{K}$ affects the residual less or the predicted measurement is trusted more.

The above formulation results in the following two-step procedure:

Prediction Step

$$\hat{\mathbf{x}}_k^- = \mathbf{A}\hat{\mathbf{x}}_{k-1} + \mathbf{B}\mathbf{u}_{k-1}$$
$$\mathbf{P}_k^- = \mathbf{A}\mathbf{P}_{k-1}\mathbf{A}^T + \mathbf{Q}_{k-1} \tag{8}$$

Update Step

$$\mathbf{K}_k = \mathbf{P}_k^- \mathbf{C}^T (\mathbf{C}\mathbf{P}_k^- \mathbf{C}^T + \mathbf{R}_k)^{-1}$$
$$\hat{\mathbf{x}}_k = \hat{\mathbf{x}}_k^- + \mathbf{K}_k (\mathbf{y}_k - \mathbf{C}\hat{\mathbf{x}}_k^-) \tag{9}$$
$$\mathbf{P}_k = (\mathbf{I} - \mathbf{K}_k\mathbf{C})\mathbf{P}_k^-$$

The Kalman filter is optimal when the model perfectly matches the real system, the entering noise is white and the noise covariances are exactly known.

At this point, it is very important to clarify the nature of the influence of the covariance matrices $\mathbf{Q}_k$, $\mathbf{R}_k$. The process noise covariance reveals the confidence put on the utilized model of the system. The lower this is, the more accurate the model is considered to be. The observation noise covariance reveals the confidence put in the acquired measurements. The lower this is, the tighter the estimator is forced to fit the recorded data. Practical implementation might be difficult when the noise covariance matrices $\mathbf{Q}_k$ and $\mathbf{R}_k$ are not known a priori which is usually the case. One approach for estimating these matrices from routine operating data is the Autocovariance Least-Squares (ALS) technique (Rajamani 2007), (Rajamani and Rawlings 2009).

2.2 The unscented Kalman Filter

The UKF is an approximation of the standard (discrete) Kalman Filter, applicable for the case of nonlinear systems. In order to simulate nonlinear behavior, the UKF approximates the state as Gaussian Random Variable (GRV), represented by a set of carefully chosen deterministic points known as Sigma Points. The Sigma Points are sample (discrete) points which are distributed so as to completely capture the true mean and covariance of the GRV and when propagated through the actual nonlinear system they capture the posterior mean and covariance accurately to the second order for any nonlinearity (third order for Gaussian inputs). If the dimension of the state vector is *L,*

then a total number of 2L+1 Sigma Points is required, as explained next. This is further illustrated in Fig. 1 for the case of a two dimensional state variable. As in the linear Kalman Filter case, a prediction and an update step is once again involved, as elaborated in what follows.

The UKF appears to be superior to the commonly used alternative approximation, the Extended Kalman Filter (EKF), especially for higher-order nonlinearities as are often encountered in civil engineering problems. The EKF in contrast, only achieves first-order accuracy. Remarkably, the computational complexity of the UKF is of the same order as that of the EKF. This section provides a basic overview of the filter equations. For more details the interested reader is referred to (Julier and Uhlmann 1997), (Wan and Van Der Merwe 2000).

Consider the general dynamical system described by the following nonlinear continuous state-space (process) equation as

$$\dot{\mathbf{x}} = \mathbf{f}(\mathbf{x}(t)) + \mathbf{w}(t) \tag{10}$$

where $\mathbf{x}(t) \in \mathfrak{R}^n$ is the state variable vector at time t, $\mathbf{w}(t)$ is the zero mean Gaussian process noise vector with covariance matrix $\mathbf{Q}(t)$.

Using numerical integration methods Eq. (10) can be rewritten as follows in discrete time

$$\mathbf{x}_{k+1} = \mathbf{F}(\mathbf{x}_k, \mathbf{w}_k) \tag{11}$$

where $\mathbf{x}_k \in \mathfrak{R}^n$ is the state variable vector at $t = k\Delta t$, $\mathbf{w}_k$ is the process noise vector with covariance matrix $\mathbf{Q}_k$, and function $\mathbf{F}$ is obtained from Eq. (10) via the integration scheme. Additionally, the nonlinear measurement (observation) equation at time $t = k\Delta t$ is

$$\mathbf{y}_k = \mathbf{h}(\mathbf{x}_k) + \boldsymbol{\upsilon}_k \tag{12}$$
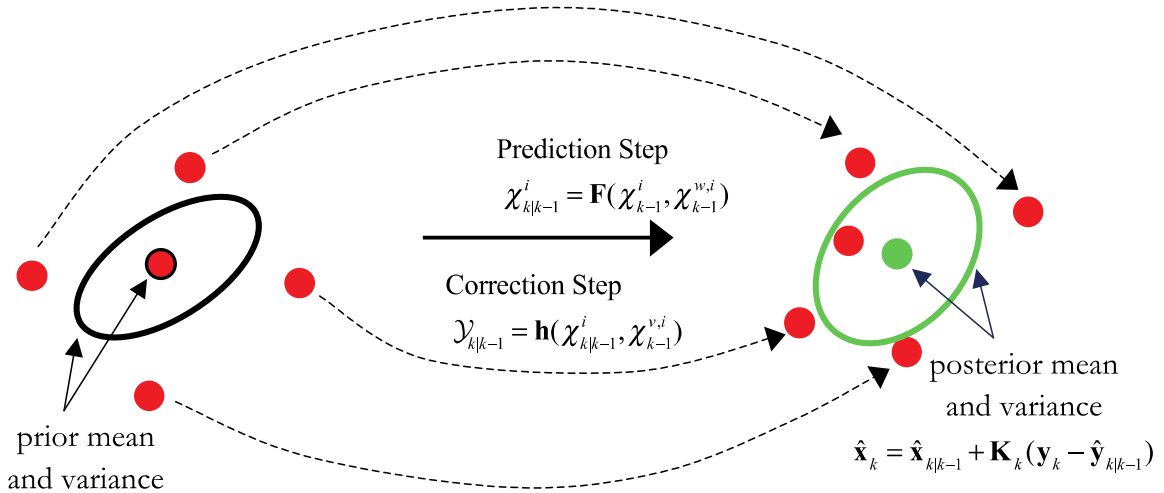

Fig. 1 Unscented Kalman Filter Visualization for 2-dimensional problem

where $\mathbf{y}_k \in \mathfrak{R}^m$ is the zero mean observation vector at $t = k\Delta t$ and $\boldsymbol{v}_k$ is the zero mean Gaussian measurement noise vector with corresponding covariance matrix $\mathbf{R}_k$.

From a Bayesian perspective, the problem of determining filtered estimates of $\mathbf{x}_k$ based on the sequence of all available measurements up to time k, $\mathbf{y}_{1:k}$ is to recursively quantify the efficiency of the estimate, by assuming different values. For that purpose, the construction of a posterior Probability Density Function (PDF) is required $p(\mathbf{x}_k \mid \mathbf{y}_{1:k})$. The UKF approximates the posterior density $p(\mathbf{x}_k \mid \mathbf{y}_{1:k})$ by a Gaussian density, which is represented by a set of deterministically chosen points. More specifically, given the state vector at step $k-1$, and assuming that this has a mean value of $\hat{\mathbf{x}}_{k-1}$ and covariance $\mathbf{P}_{k-1}$, we can calculate the statistics of $\mathbf{x}_k$ by using the Unscented Transformation, or in other words by computing the set of $2L+1$ sigma points χ_k^i with associated weights W_i.

In order to do so, the original state vector is redefined as the concatenation of the original state vector and noise variables as $\mathbf{x}_{k-1}^\alpha = [\mathbf{x}_{k-1}^T \ \mathbf{w}_{k-1}^T \ \boldsymbol{v}_{k-1}^T]^T$. Then, the Sigma Points are distributed symmetrically around the mean $\hat{\mathbf{x}}_{k-1}^\alpha$ as follows

$$
\begin{aligned}
\chi_{k-1}^\alpha &= \left[(\chi_{k-1})^T \quad (\chi_{k-1}^w)^T \quad (\chi_{k-1}^v)^T \right] = \\
&= \hat{\mathbf{x}}_{k-1}^\alpha \quad \hat{\mathbf{x}}_{k-1}^\alpha + \sqrt{(L+\lambda)\mathbf{P}_k^\alpha} \quad \hat{\mathbf{x}}_{k-1}^\alpha - \sqrt{(L+\lambda)\mathbf{P}_k^\alpha} \,]
\end{aligned}
\tag{13}
$$

where $P_k^\alpha \in \mathbb{R}^{L \times L}$ is the corresponding augmented covariance matrix incorporating the process and observation noise components: $\mathbf{P}^\alpha = diag(\mathbf{P}, \mathbf{Q}, \mathbf{R})$. L is the dimension of the augmented state estimate vector $\hat{\mathbf{x}}_{k-1}$, $(\alpha, \ \kappa, \ \beta)$ are the KF parameters, and $\lambda = \alpha^2(L+\kappa) - L$ is a scaling parameter. For further details, one may refer to (Wan and Van Der Merwe 2000), (Ristic *et al.* 2004).

These Sigma Points are propagated through the original nonlinear system function $\mathbf{F}(\mathbf{x}_k)$

$$
\chi_{k|k-1}^i = F(\chi_{k-1}^i, \chi_{k-1}^{w,i}), \quad i = 0, \dots, 2L
\tag{14}
$$

where L is the dimension of the state vector $\mathbf{x}$.

The set of the sample points $\chi_{k|k-1}^i$ represents the predicted density $p(\mathbf{x}_k \mid \mathbf{y}_{1:k-1})$. Consequently, the mean and covariance of the state at time step k are approximated using a weighted sample mean and covariance of the posterior Sigma Points. Under this assumption, a variation of the standard Kalman Filter process can be enforced. This consists in a two-stage evaluation comprising a time-update step and a measurement-update step. The time-update is executed as follows

$$
\hat{\mathbf{x}}_{k|k-1} = \sum_{i=0}^{2L} W_i^m \chi_{k|k-1}^i
\tag{15}
$$

$$P_{k|k-1} = \sum_{i=0}^{2L} W_i^c \left[\chi_{k|k-1}^i - \hat{X}_{k|k-1} \right] \left[\chi_{k|k-1}^i - \hat{X}_{k|k-1} \right]^T \qquad (16)$$

Note that the notation $\Big|_k^{-}$ used previously is identical to the notation $\Big|_{k|k-1}$ used here for convenience. Moreover, the weights for the state and covariance components of the Sigma Point vector are given in the following relation

$$W_0 = [W_0^m \ W_0^c] = \left[\frac{\lambda}{L+\lambda} \ W_0^m + (1 - \alpha^2 + \beta) \right]$$

$$W_i^c = W_i^m = \frac{1}{2(L+\lambda)}, \ i = 1,\ldots,2L \qquad (17)$$

The predicted measurement mean and covariance are then equal to

$$\mathcal{Y}_{k|k-1} = \mathbf{h}(\chi_{k|k-1}^i, \chi_{k-1}^{v,i}) \qquad (18)$$

$$\hat{\mathbf{y}}_{k|k-1} = \sum_{i=0}^{2L} W_i^m \mathrm{Y}_{k|k-1}^i \qquad (19)$$

$$\mathbf{P}_k^{yy} = \sum_{i=0}^{2L} W_i^c [\mathcal{Y}_{k|k-1}^i - \hat{\mathbf{y}}_{k|k-1}][\mathcal{Y}_{k|k-1}^i - \hat{\mathbf{y}}_{k|k-1}]^T \qquad (20)$$

The second stage of the estimation, termed the measurement-update step, takes place as follows

$$\hat{X} = \hat{X}_{k|k-1} + K_k(y_k - \hat{y}_{k|k-1}) \qquad (21)$$

$$\mathbf{P}_k = \mathbf{P}_{k|k-1} - \mathbf{K}_k \mathbf{P}_k^{yy} \mathbf{K}_k^T \qquad (22)$$

where $\mathbf{K}_k$ is the Kalman Gain matrix at step k

$$\mathbf{K}_k = \mathbf{P}_k^{xy} (\mathbf{P}_k^{yy})^{-1} \qquad (23)$$

$$P_k^{xy} = \sum_{i=0}^{2L} W_i^{(c)} \left[\chi_{k|k-1}^i - \hat{X}_{k|k-1} \right] \left[y_{k|k-1}^i - \hat{y}_{k|k-1} \right]^T \qquad (24)$$

2.3 Multi-rate Kalman Filter

When fusion of signals sampled at different rates is required, a multi-rate formulation of the UKF can be utilized. Let us assume availability of acceleration and displacement signals, sampled at different intervals, T_a, T_d, respectively where $T_d / T_a = M$, $M \in \mathrm{N}$. A multi-rate Kalman

filter can be applied to obtain the optimal estimates of the displacement and velocity. Since no displacement measurements are available between the times kT_d, where k is an integer, this is equivalent to optimal filtering with arbitrarily large measurement errors. Consequently, the measurement covariance related term appearing in Eq. (12) of the Measurement Update step (Fig. 1), $\mathbf{P}_{yy}^{-1}$ is arbitrarily large and hence the Kalman gain $\mathbf{K} \to 0$. Thus, only the time update is performed and the optimal estimate is

$$\hat{X}_{k+1} = \hat{X}_{k+1}^{-} = E(\chi_{k+1|k})$$

$$P_{k+1} = P_{k+1}^{-} = Var(\chi_{k+1|k}) \tag{25}$$

When displacement measurements become available, at time instants kT_d, both the time and measurement update are regularly performed. It is important to note however that even when implementing such a scheme, displacement estimates can still drift particularly for larger sampling ratios. Smoothing techniques can help tackle this problem; however their efficacy largely depends upon data quality and noise content. In addition, the use of smoothing calls for a non-causal procedure as described next, which is not ideal for online implementations.

2.4 Kalman filter smoothing

Smoothing can produce improved estimates of the state by processing a window of the response, i.e., no longer relying solely on the previous and current state (Markov assumption). Smoothing works through a combination of the forward Kalman filtering and backward filtering over the entire sequence of available measurements and is therefore an off-line procedure. In the second application presented herein, an Unscented Rauch-Tung-Striebel (RTS) smoother is appied for performance evaluation purposes. The original RTS algorithm was introduced by Rauch in 1965 (Rauch *et al*. 1965), however the formulation described in (Sarkka 2008), (Terejanu *et al*. 2007) is adopted here for coupling this concept with the UKF. Following this approach, smoothing is accomplished by first filtering up to the current measurement and then sweeping back a fixed number of steps with the RTS algorithm. If the number of backward steps S is small, then the state estimation is "near online". The smoothed estimates $\hat{\mathbf{x}}_k^s$ over the interval $(T - S, T)$ can be obtained by

$$\hat{\mathbf{x}}_k^s = \hat{\mathbf{x}}_k + \mathbf{K}_k^s \left(\hat{\mathbf{x}}_{k+1}^s - \hat{\mathbf{x}}_{k+1}^- \right)$$

$$\mathbf{P}_k^s = \mathbf{P}_k - \mathbf{K}_k^s \left(\hat{\mathbf{P}}_{k+1}^- \hat{\mathbf{P}}_{k+1}^s \right) \left(\mathbf{K}_k^s \right)^T \tag{26}$$

Where $\hat{\mathbf{x}}_k^s$ is the updated state estimate from the forward filter, while the smoothing gain $\mathbf{K}_k^s$ is defined as

$$K_k^s = P_{k+1|k} \hat{x}_{k+1}^- (P_{k+1}^-)^{-1} \tag{27}$$

The purpose of this work is to demonstrate how the use of schemes of this type can in fact be overruled, so that the simulation is maintained at the lowest possible computational cost, yielding

it suitable for real-time implementation.

3. Artificial white noise observations

In an effort to track the state evolution in real-time while alleviating the "drift effect", a concept relevant to the approach described in the (Kim *et al.* 2014) is introduced herein. In the cases examined by Kim et al. availability of collocated displacement measurements is assumed and a multi-rate Kalman filter is enforced. The acceleration measurement error is considered as a combination of offset bias (e.g., mechanical or electrical hysteresis and accelerometer installation errors) and a zero-mean stochastic noise process. The filter equations are formulated by setting the state variables of the Kalman filter as the acceleration error and its single and double integrators, i.e., velocity and displacement integration errors, respectively. This approach proves efficient for the problem of fusing collocated displacement and acceleration measurements although, as noted by the authors, the "drift effect" is once again present and a smoother is utilized for its correction.

In the method introduced herein, the more generalized cases of non-collocated acceleration and displacement data; and of pure acceleration (no displacement) records are investigated. In this approach, modification of the filter equations lies in the appropriate expansion of the observation equation set in order to include a set of artificial zero-mean White Noise (WN) observations $\mathbf{y}_k^\alpha$ for the unobserved displacement states $\mathbf{x}_k^u \in \mathbb{R}^l$

$$\mathbf{y}_k^\alpha = \mathbf{x}_k^u + \boldsymbol{\upsilon}_k^\alpha \tag{28}$$

where $\mathbf{y}_k^\alpha = \mathbf{0}_{l \times 1}$ is the artificial observation value, set to zero, and $\boldsymbol{\upsilon}_k^\alpha$ is the noise level assumed for these artificial observations. It is reminded at this point that a very low level would indicate confidence in this false measurement, which is undesirable. The target is to maintain the mean at a zero level while not overriding the system model estimates. In this way detrending is essentially executed in an online manner. Therefore, higher noise amplitudes should be attributed to these observations as indicated next.

3.1 Illustration on the integration of a noisy acceleration signal

In order to demonstrate the influence of the artificial observations terms, the toy-example of numerical integration for the acceleration response of a single degree of freedom (sdof) linear oscillator is explored next. The properties of the oscillator, which is schematically shown in Figure 2a, are set as $k = 900$ N/m, $m = 100$ kgr, $c = 25$ Ns/m. A record of the 1994 Northridge earthquake (Fig. 2(b)), scaled at a peak acceleration of .3 g, is used as the input base excitation, simulating an sdof system under earthquake excitation. The noise-free ("clean") system is numerically simulated for a total duration of 20 sec and the response acceleration is contaminated with white noise of different levels as defined by their Root-Mean-Square (RMS) noise to signal ratio. The RMS is a statistical measure of the magnitude of a time history. It is reminded here, that for discrete signals, the RMS ratio is defined as the square root of the ratio of the sums of squared components for each time signal. A sampling frequency of 200 Hz is utilized in this example.

(a) Single degree of freedom, linear oscillator   (b) The Northridge Earthquake (unscaled)
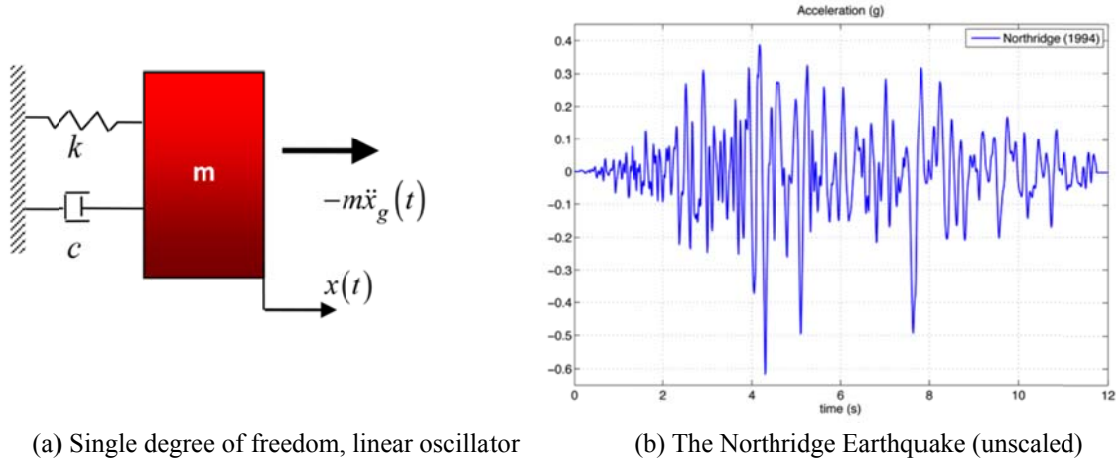
Fig. 2 System setup and input motion

Next, three separate approaches are implemented for numerically integrating the obtained response in an effort to derive the displacement response record:

1. Numerical integration using a 4th order Runge Kutta (RK) scheme
2. Filtering approach using the standard (linear) Kalman Filter (KF)
3. Filtering approach using the Unscented Kalman Filter (UKF)

The purpose of using both the KF and the UKF is for demonstrating the higher versatility of the UKF in handling different noise levels. Fig. 3 demonstrates the performance of the ode45 method for a 2% RMS additive noise, with and without detrending. Note that detrending is not only suboptimal, but additionally is unsuitable for real-time implementation, as it involves processing of the whole data record or a significant portion of it. Also, note that the drift effect is more significant on displacement than it is on the velocity estimates.

Subsequently, a filtering approach is enforced using the following state-space (process) equation

$$\dot{\mathbf{x}}(t) = \begin{bmatrix} 0 & 1 \\ 0 & 0 \end{bmatrix} \mathbf{x}(t) + \begin{bmatrix} 0 \\ \ddot{x}_m(t) \end{bmatrix} + \mathbf{w}(t) = \mathbf{A}\mathbf{x}(t) + \mathbf{B}\mathbf{u}(t) + \mathbf{w}(t) \qquad (29)$$

where $\mathbf{x}(t) = [x(t)\ \dot{x}(t)]^T$ is the state vector of the system; $\mathbf{u}(t) = \ddot{x}_m(t)$ is the noise corrupted recorded acceleration signal; and $\mathbf{w}(t)$ is the process noise, of covariance $Q = 1e-6$. Prior to implementing the filtering scheme, the continuous state-space equation is discretized as follows

$$\mathbf{x}_{k+1} = \mathbf{A}_d \mathbf{x}_k + \mathbf{B}_d \mathbf{u}_k + \mathbf{w}_k \qquad (30)$$
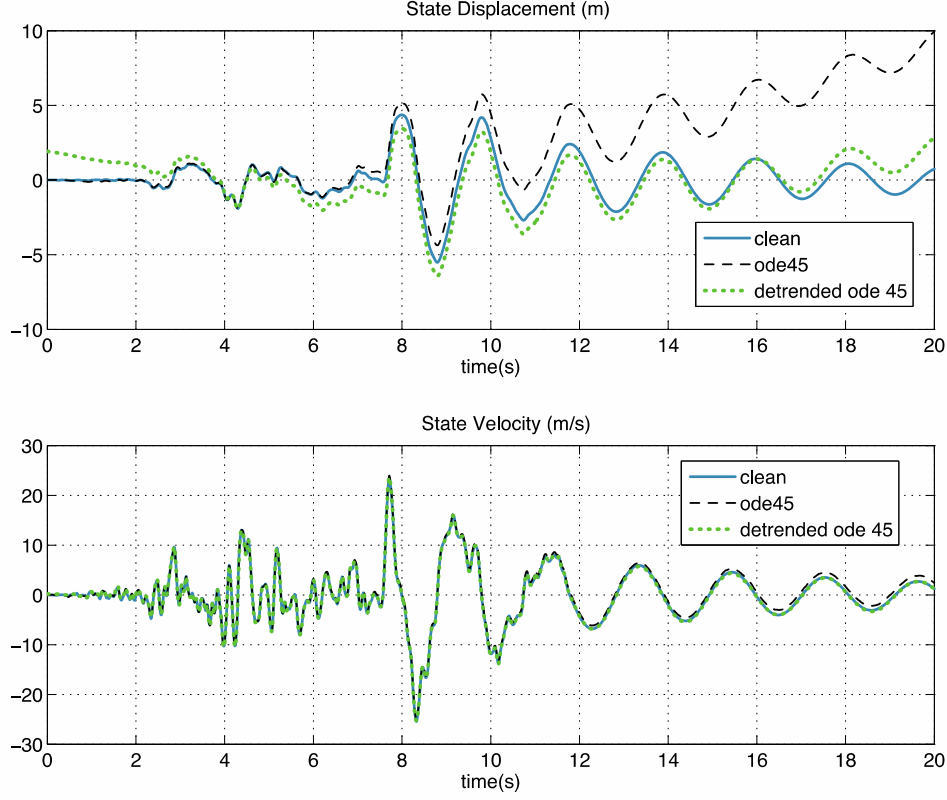
Fig. 3 Integrated Displacement and Velocity using the RK method

where since the continuous system matrix $\mathbf{A}$ is nilpotent, i.e., $\mathbf{A}^2 = 0$, it follows that

$$
\begin{aligned}
\mathbf{A}_d &= e^{\mathbf{A}\Delta t} = \mathbf{I} + \mathbf{A}\Delta t \\
\mathbf{B}_d &= \left(\int_0^{\Delta t} e^{\mathbf{A}\tau} d\tau \right) \mathbf{B} = \left(\mathbf{I}\Delta t + \frac{1}{2!} \mathbf{A}\Delta t^2 \right) \mathbf{B}
\end{aligned}
\tag{31}
$$

The above state-space equation is complemented by an artificial observation $y_k^\alpha = 0$ as formerly introduced in Eq. (28)

$$
y_k^\alpha = x_k + \upsilon_k^\alpha
\tag{32}
$$

The results for displacement are displayed in Fig. 4 for varying levels of the RMS ratio of the noise process υ^α to the displacement signal. It is reminded at this point, that this is an illustrative example which helps demonstrate the workings of this scheme on the simple integration of a noisy acceleration signals without assuming availability of supplemental measurements, such as displacement as in (Smyth and Wu 2007), (Kim *et al.* 2014). As observed in Fig. 4, when the noise

covariance of the artificial observation is kept at a very low level (a), the filter forces the model to adhere to the false, zero observation, leading to an incorrect estimate for both the KF and UKF approach. However, once the noise level is a bit relaxed (b) this effect is relaxed as well leading the solution closer to what is dictated by the model (i.e., the integrator). In fact in subfigure (b) the noise level is such that the linear KF achieves a very good prediction of the integrated displacement. The UKF performance is improved but still distorted by the tighter confidence on the artificial observation. Further relaxation (c), (d) of the noise level assigns less weight on the artificial observation which leads the linear KF to diverge, as it is essentially now operating solely on the grounds of the process equation (state-space).

Unlike the linear KF, the UKF consistently provides an improved estimate of the displacement for increasing noise levels, with optimal performance for the noise RMS noise to signal ratio lying within the range of .5 to 50. This demonstrates the greater versatility of the UKF versus the KF in the proposed scheme, which is why in what follows the UKF will be used for all simulations (both linear and nonlinear). It is worth noting here that it is not possible to predefine the optimal value of the υ^{α} noise level to be used. What is important however is that the method works for a wide range of such values, usually above some lower threshold and not for one unique optimal. This renders the method easily applicable without a need for extensive fine-tuning. As aforementioned in Section 2.1, the same holds for the process and observation noise levels of the linear KF, which are typically defined from existing (routine) data.
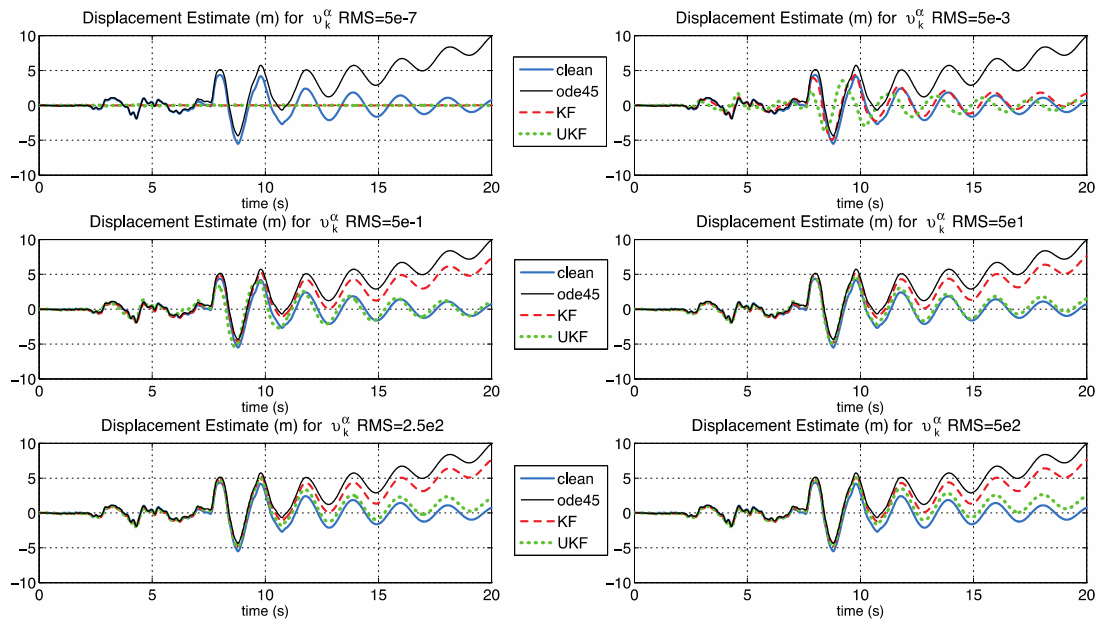

Fig. 4 Integrated Displacement using the RK, the linear KF, and the Unscented KF methods for different noise levels

A second note lies in the following; in the case of permanent deformations, which could sometimes be the result of nonlinearity, this method would not be applicable in this form. The current formulation only applies for cases where vibration takes place around the same equilibrium position y=0, which is however quite often the case. The method could be expanded to potentially account for permanent deformation, and therefore shifts in the mean value of the specified noise level, however this is left as future work.

In what is discussed above, no information on the actual model of the system is included in the state-space formulation and no additional reliable observation is assumed. As is demonstrated in the following section, results are significantly improved when additional information is incorporated into the analysis process.

4. Single degree of freedom numerical example

4.1 Sdof linear oscillator with known system model - state identification

In this section, we take the analysis one step further, by taking the dynamic equation of motion into account for the formulation of the state-space (process) equations. A single degree of freedom oscillator is once again considered (Fig. 2(a)) with known structural properties: $k = 900$ N/m, $m = 100$ kgr, $c = 25$ Ns/m. A sampling rate of 200 Hz is utilized all through this example. The continuous system now assumes the following form

$$\dot{\mathbf{x}}(t) = \begin{bmatrix} 0 & 1 \\ -m^{-1}k & -m^{-1}c \end{bmatrix} \mathbf{x}(t) - \begin{bmatrix} 0 \\ 1 \end{bmatrix} \ddot{x}_g(t) + \mathbf{w}(t) = \mathbf{A}\mathbf{x}(t) + \mathbf{B}\mathbf{u}(t) + \mathbf{w}(t) \tag{33}$$

where $\mathbf{x}(t) = [x(t) \ \dot{x}(t)]^T$ is the state vector of the system; $\ddot{x}_g(t)$ is the noise corrupted (5% RMS ratio) input ground motion (scaled record of Northridge earthquake); and $\mathbf{w}(t)$ is the process noise, of covariance $Q = 1e-8$. The continuous system is discretized using a simple forward Euler integration scheme at a sampling frequency of 200 Hz. Measurements of the total acceleration are once again assumed available, contaminated with considerable noise of 15% RMS ratio. The relevant observation equation then becomes

$$y(t) = \ddot{x}_m(t) = -1/m(kx(t) + c\dot{x}(t)) + \upsilon(t) \tag{34}$$

As indicated by the performance of the estimator (Fig. 5), taking the underlying system model into account, resolves the drift issue even at quite increased noise levels. However, this is not the case when uncertainty in the structural properties is involved, as examined next.

4.2 Sdof linear oscillator with uncertain system model - Joint state & parameter identification

Once again we gradually increase the complexity of the problem considered, this time taking model uncertainty into account. More specifically, the system properties are assumed unknown a priori and their online identification is sought during acquisition, rendering this a joint state and parameter identification problem. We therefore assume that the k/m, c/m values are to be

estimated online. The previous formulation can easily be brought into a joint identification form by augmenting the state vector in order to include the unknown parameter vector $\boldsymbol{\theta} = [k \; c]^T$

$$\dot{\mathbf{x}}(t) = \begin{bmatrix} x(t) \\ -m^{-1}kx(t) - m^{-1}c\dot{x}(t) \\ 0 \\ 0 \end{bmatrix} - \begin{bmatrix} 0 \\ 1 \\ 0 \\ 0 \end{bmatrix} \ddot{x}_g(t) + \mathbf{w}(t) = \mathbf{f}\tilde{\mathbf{x}}(t) + \mathbf{B}\mathbf{u}(t) + \mathbf{w}(t) \qquad (35)$$

where $\tilde{\mathbf{x}}(t) = [x(t) \; \dot{x}(t) \; k \; c]^T$ is now the augmented state vector of the system which inevitably results in a nonlinear system function $\mathbf{f}$, due to the bilinear products of state components ($m^{-1}kx(t)$, $m^{-1}c\dot{x}(t)$). The implementation of a nonlinear system identification method is therefore mandatory in this case. The observation Eq. (34) is once again utilized and an off-assumption of initial conditions $k / m \big|_0 = 6$, $c / m \big|_0 = 0.5$ is made. As illustrated in Figs. 6 and 7 the performance of the filter is now suboptimal. An initial integration error is clearly marked in the first seconds of the analysis, leading to the identification of erroneous system parameters, which subsequently worsens state tracking as well. The influence of the "drift effect" is obvious throughout the estimation. It needs to be noted that the filter is able to accurately track the measured (observed) acceleration, as demonstrated in Fig. 8, however the errors inserted into the process equation, i.e., the state-space formulation through integration, generate this inferior performance.
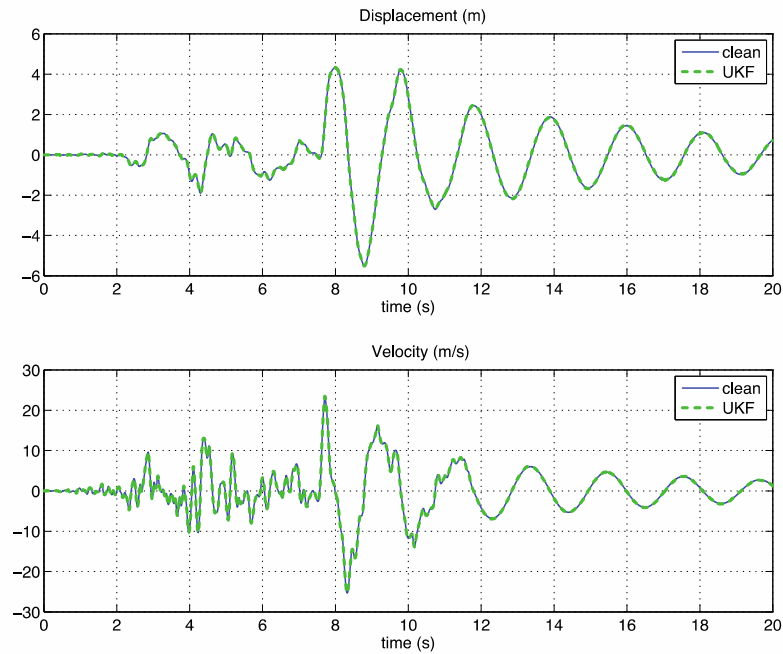

Fig. 5 State estimates using the Unscented KF for known linear system model
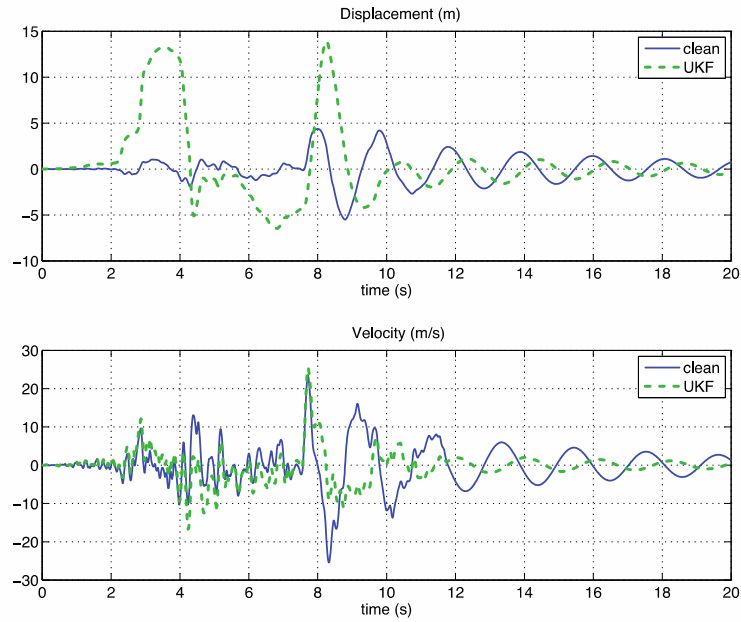
Eleni N. Chatzi and Clemente Fuggini

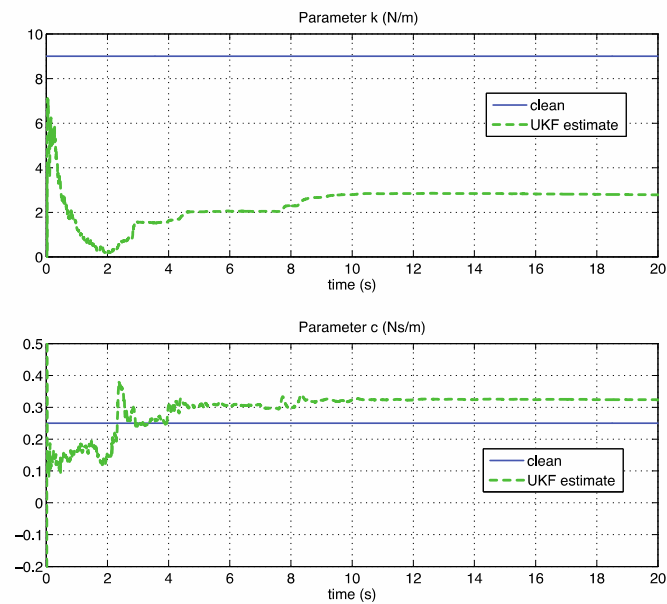Fig. 6 State estimates using the Unscented KF for uncertain linear system model

Fig. 7 Parameter estimates using the Unscented KF for uncertain linear system model
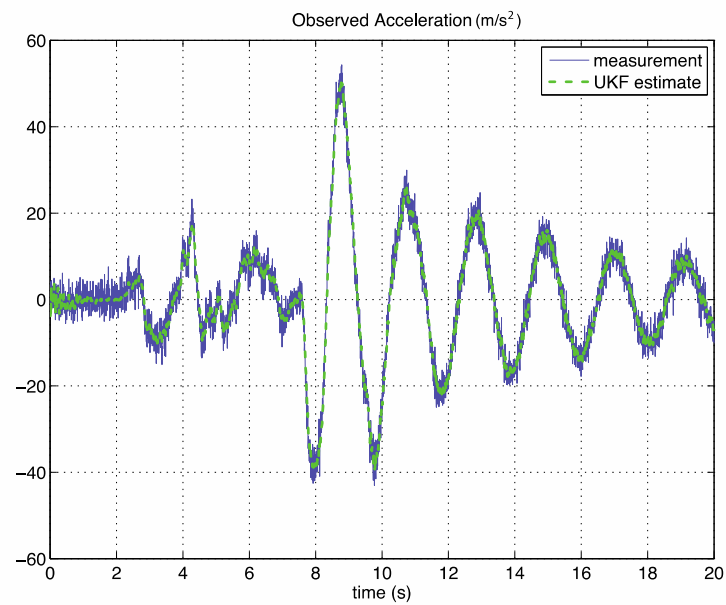
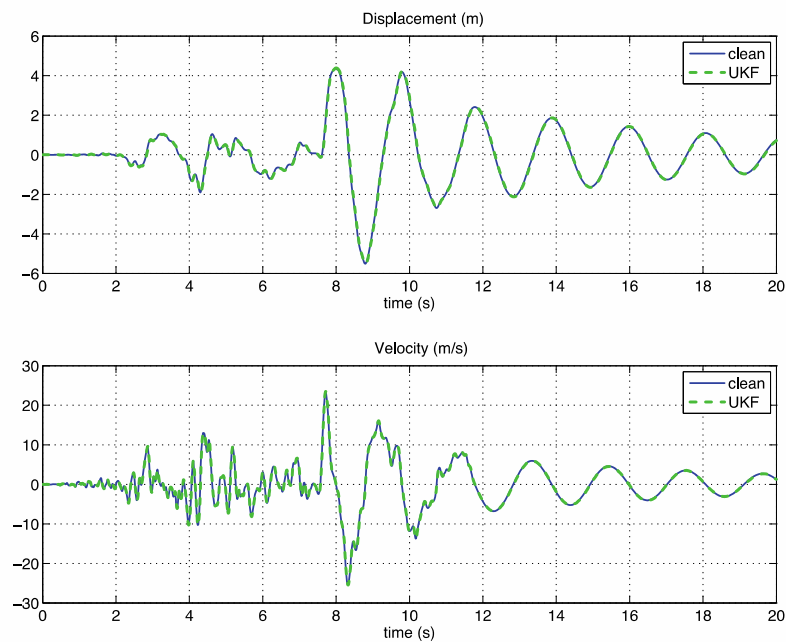Fig. 8 Observation tracking using the Unscented KF for uncertain linear system model

Fig. 9 State estimates using the Unscented KF for uncertain linear system model and artificial observations

The same system is now modified through the addition of the artificial white noise observation, y^α, of Eq. (32) using a covariance $R = 0.1$

$$\mathbf{y}(t) = \begin{bmatrix} \ddot{x}_m(t) \\ y^\alpha(t) \end{bmatrix} \begin{bmatrix} -1/m(kx(t) + c\dot{x}(t)) \\ x(t) \end{bmatrix} + \begin{bmatrix} \upsilon(t) \\ \upsilon^\alpha(t) \end{bmatrix} \tag{36}$$

As observed in Figs. 9 and 10 the system now converges to the true parameter values, while achieving an accurate tracking of structural response. The converged damping parameter estimate is somewhat deviating from the exact value, however this is a known issue in damping parameter identification and the divergence level observed here is not significant. Furthermore, as pointed out earlier in Section 3.1, the convergence is not really sensitive on the choice of this covariance level, provided it is not too low. It is reminded that a very low value would force the signal to adhere to this fictitious observation, which is of course undesirable.
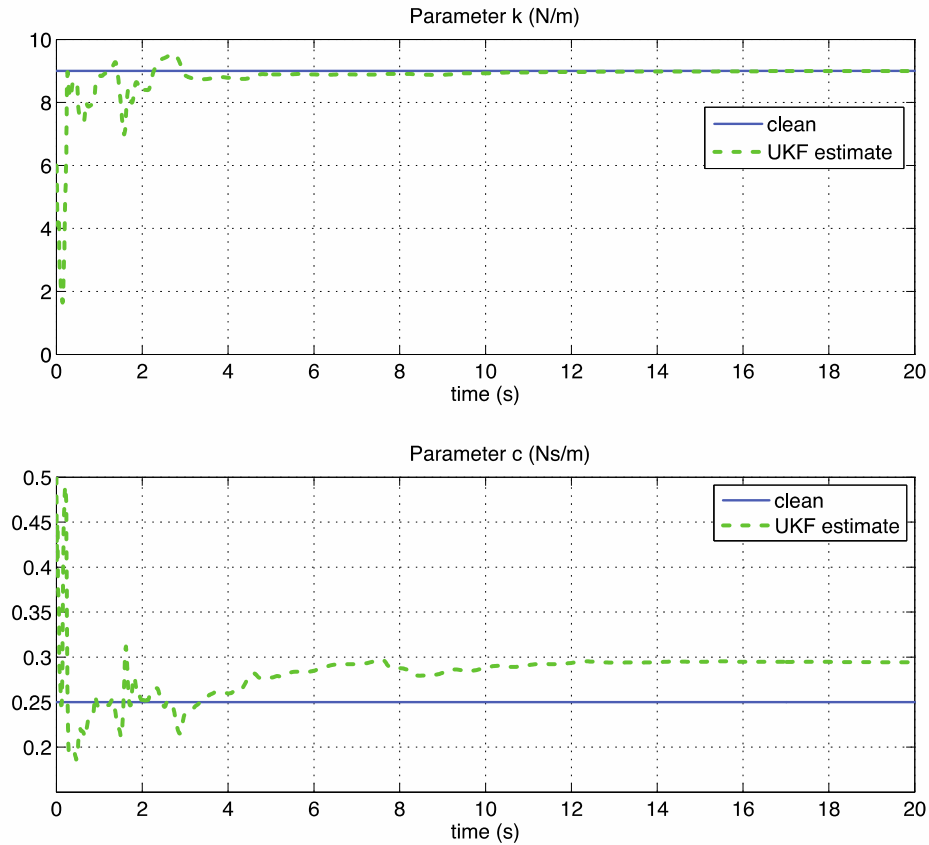

Fig. 10 Parameter estimates using the Unscented KF for uncertain linear system model and artificial observations
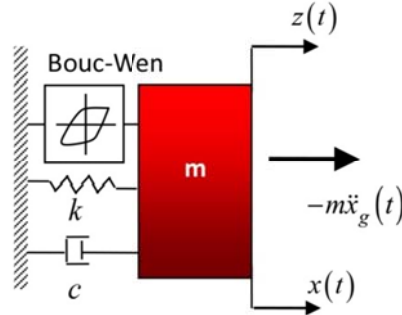
Fig. 11 Single degree of freedom, nonlinear oscillator with hysteresis

4.2 Sdof nonlinear oscillator with uncertain system model - Joint state & parameter identification

Finally, in order to explore a further level of complexity, the previous system is modified by considering nonlinear hysteretic behavior for the oscillator (Fig. 11). A Bouc–Wen type model is utilized for the modeling of hysteresis as it is particularly suited for a state-space formulation.

The resulting nonlinear system calls for an increase of the original system's states through the addition of a hysteretic degree of freedom $z(t)$ while the parameter vector is also extended to include the Bouc–Wen parameter set $\boldsymbol{\theta}_{BW} = [\beta \ \gamma \ n]^T = [2 \ 1 \ 2]^T$. The aim is to once again perform joint state and parameter identification and the state-space equations are reformulated as follows

$$\dot{\tilde{\mathbf{x}}}(t) = \begin{bmatrix} x(t) \\ \dot{x}(t) - \beta |\dot{x}(t)| z(t) |z(t)|^{n-1} - \gamma \dot{x}(t) |z(t)|^n \\ -m^{-1}kz(t) - m^{-1}c\dot{x}(t) \\ \mathbf{0}_{5x1} \end{bmatrix} - \begin{bmatrix} 0 \\ 0 \\ 1 \\ \mathbf{0}_{5x1} \end{bmatrix} \ddot{x}_g(t) + \mathbf{w}(t) \Rightarrow \qquad (37)$$

$$\dot{\tilde{\mathbf{x}}}(t) = \mathbf{f}\left(\tilde{\mathbf{x}}(t)\right) + \mathbf{B}\mathbf{u}(t) + \mathbf{w}(t)$$

where $\tilde{\mathbf{x}}(t) = [x(t) \ z(t) \ \dot{x}(t) \ k \ c \ \beta \ \gamma \ n]^T$ is now the augmented state vector of the system which once again results in a nonlinear system function $\mathbf{f}$. The input excitation, and process noise levels are kept the same as in the previous cases whereas an off-assumption of initial conditions, $k/m|_0 = 6$, $c/m|_0 = .5$, $\beta|_0 = 3$, $\gamma|_0 = 2$, $n|_0 = 1$ is made. The analysis is once again performed without and with the artificial WN observation assumption, i.e., according to Eqs. (25) and (27) respectively. The results for the state and parameter estimates are illustrated in Figs. 12-14, where the improvement of the prediction is shown to be even more notable in the nonlinear case. It is obvious that the original system, operating in absence of the artificial WN observation, fails to converge, especially during the first seconds of the analysis where larger nonlinearities occur due to increased loading levels.
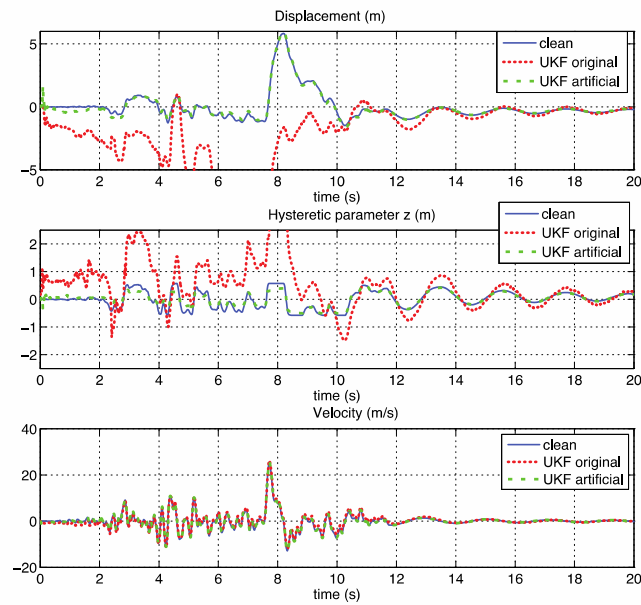
Fig. 12 State estimates using the Unscented KF for uncertain nonlinear system model both with and without artificial observations
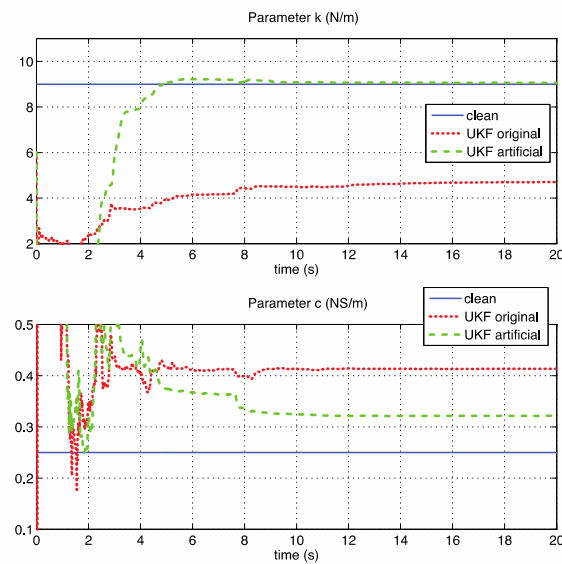

Fig. 13 Stiffness and damping parameter estimates using the Unscented KF for uncertain nonlinear system model both with and without artificial observations
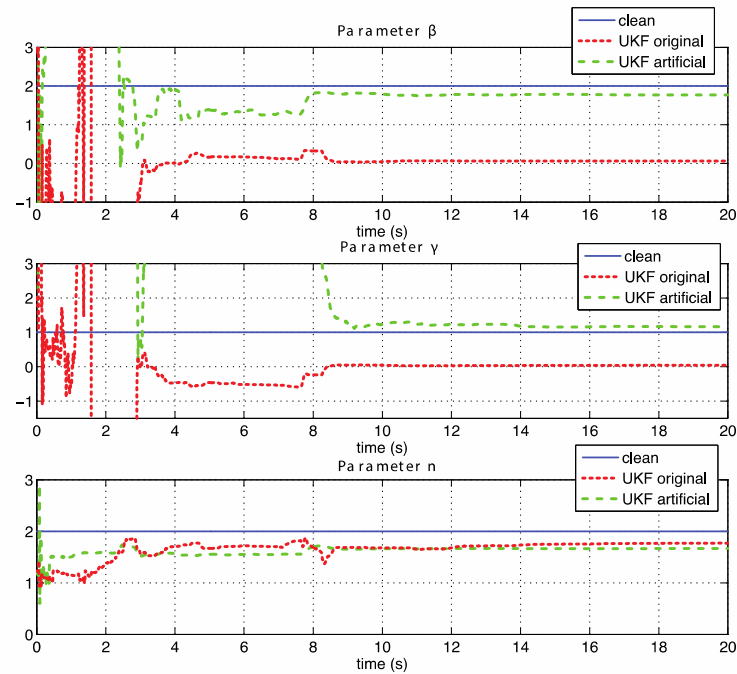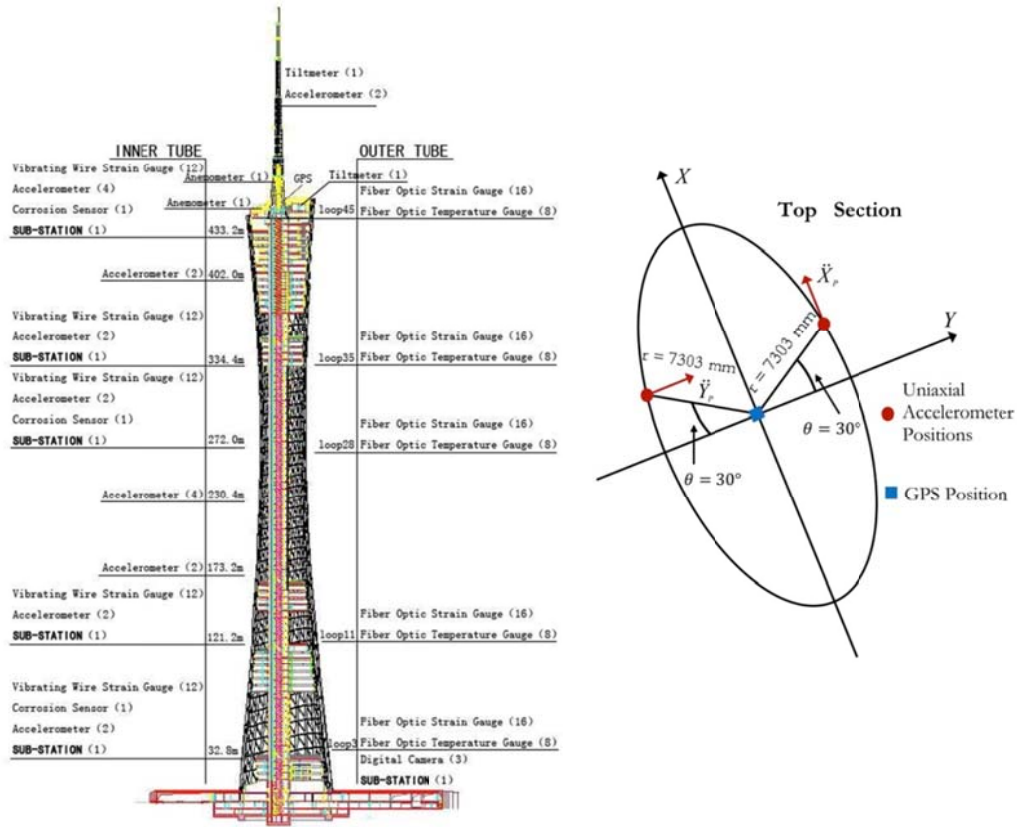
Fig. 14 Bouc-Wen model parameter estimates using the Unscented KF for uncertain nonlinear system model both with and without artificial observations

5. Large scale structure inspired application

The previous example demonstrated the efficacy of the proposed method in the presence of acceleration measurements alone. However, it is interesting to additionally point out its effectiveness for the fusion of displacement and acceleration records. For this purpose an actual high-rise structure in China, the Guangzhou TV tower, is chosen as the test case for this second application. A dense monitoring system, comprising over 700 sensors (Fig. 15(a)), has been implemented on the 610 m tall structure, by the Hong Kong Polytechnic University for both in-construction and in-service real-time monitoring. A number of interesting works have been conducted concerning the modal identification of the structure under ambient loading using a stochastic subspace identification (SSI-data) approach (Faravelli *et al*. 2011), (Faravelli *et al*. 2010a), (Faravelli *et al*. 2010b). Additionally, in previous work by Fuggini (2009), Casciati *et al*. (2009), and Faravelli *et al*. (2009), the issue of fusing GPS information with non-collocated accelerometer data for the identification of the torsional response at the top section of the tower was investigated.

In the current work, the computational technique introduced earlier is employed on a numerically simulated case of the aforementioned tall-tower torsion problem. This example is of particular interest since it calls for the fusion of heterogeneous data, sampled at different rates as in the works of (Smyth and Wu 2007), (Kim *et al*. 2014).

(a) Photo from: http://www.cse.polyu.edu.hk/benchmark/   (b) GPS and accelerometer sensors)

Fig. 15 (a) Actual tower instrumentation pattern and (b) Location of the assumed measurement points for both

As mentioned in Casciati *et al.* (2009) and Fuggini (2009), the moving GPS was placed in the center of the oval section, while the two accelerometers were placed at the edges of this section, one along the East-West direction and the second along the North-South direction as shown in Fig. 15(b). All were placed at a 443 m height level. The reference GPS receiver was fixed at the ground level at a distance from the tower sufficient to prevent any multipathing effects. It is assumed - as plotted in Fig. 15(b) - that the X and Y axes are respectively the directions along the long axis and the short axis of the oval cross section. Therefore the X-direction measurements obtained from the accelerometers correspond to the North coordinates of the GPS measuring system; while measurements in the Y-direction correspond to the East coordinates, as clarified in Fig. 15(b).

For the purposes of the application considered here, we rely on a set of numerically generated data, of characteristics similar to the strong wind event cases as these are presented in previous works on this structure (Casciati *et al.* 2009, Faravelli *et al.* 2010a). These serve as the input information in order to assess the torsional angle by which the upper in-plane section of the tower is rotated. The GPS sampling rate is assumed equal to 5 Hz, while the sampling rate of the two

uni-axial accelerometers is set to 50 Hz, as indeed was the case on the actual structure.

5.1 Governing geometric relations

In order to detect the torsional behavior of the tower, the geometric formulas for an oval cross-section must be set up. In the considered case study the GPS receiver is placed at the center of the oval inner tube, and the two uniaxial accelerometers are located at a distance r from the center, while the accelerometer position vector forms an angle θ with the Y axis (Fig. 15(b)). The GPS receivers measure the displacements at the center of the cross-section in the two horizontal directions. The data collected from both the accelerometers at the far edges of the inner tube of the tower and the GPS receiver at the center of the section, shall allow for the tracking of the torsional response. The in-plane displacements, Δx and Δy, due to the pure rotation of the cross-section are simply calculated by subtracting the displacements obtained at the center from the one simultaneously measured at the edges, as follows

$$\Delta x = X_p - X_0, \Delta y = Y_p - Y_0 \tag{38}$$

where X_0 and Y_0 are the displacements measured by the GPS receiver, and X_p and Y_p are the displacements calculated from the accelerometer records in the corresponding directions. Based on the geometry described in Figure 16, the following geometric relations hold

$$\begin{aligned} r\cos(\theta - \varphi) &= r\cos\theta - \Delta y \\ r\sin(\theta + \varphi) &= r\sin\theta + \Delta x \end{aligned} \tag{39}$$

By rearranging the two formulas in Eq. (38), the angle of rotation, ϕ, can be calculated from either one of the two in-plane displacements

$$\begin{aligned} \varphi &= \theta - \cos^{-1}\left(\cos\theta - \frac{\Delta y}{r}\right) \\ \varphi &= \sin^{-1}\left(\sin\theta + \frac{\Delta x}{r}\right) - \theta \end{aligned} \tag{40}$$

For the considered case-study, the values of r and θ are equal to 7303 mm and 30°, respectively, as specified in Fig. 15(b).

In previous work (Casciati *et al.* 2009), numerical integration and filtering was used in order to obtain the displacement time histories recorded by the accelerometers for both directions X and Y. Since the GPS and the accelerometer signals are independently recorded, a suitable synchronization is strongly needed in order to perform a comparative analysis. As can be inferred from Eqs. (40), two independent expressions exist for the evaluation of the angle of rotation ϕ. However, the measurement signals X_0, Y_0 originating from the GPS can come with imprecisions relating to the geometric dilution of precision (GDOP). In addition, the X_p, Y_p estimates are obtained through filtering and numerical integration, therefore we expect to obtain diverging ϕ estimates from the above independent equations. Depending on the noise level these

may in fact vary quite significantly.

5.2 State-space formulation

The process implemented herein, enabled by the use of a Multirate-Unscented-Kalman Filter, takes advantage of the redundancy of the two geometric relations in order to correlate the different recordings and to ultimately obtain an estimate of improved accuracy. In order to implement the filter, we need to first bring the system into state-space form. This is achieved by assuming the following state vector

$$x = \begin{bmatrix} X_p & Y_p & \dot{X}_p & \dot{Y}_p \end{bmatrix}^T \tag{41}$$

where X_p, Y_p correspond to the dofs of the accelerometer nodes in directions x and y respectively. Then, considering that the nodal accelerations $\ddot{X}_p$, $\ddot{Y}_p$ are measured, the process equation can be modeled in state-space equation form

$$\dot{x} = \begin{bmatrix} \dot{X}_p \\ \ddot{X}_p \\ \dot{Y}_p \\ \ddot{Y}_p \end{bmatrix} = \begin{bmatrix} 0 & 1 & 0 & 0 \\ 0 & 0 & 0 & 0 \\ 0 & 0 & 0 & 1 \\ 0 & 0 & 0 & 0 \end{bmatrix} \begin{bmatrix} x_1 \\ x_2 \\ x_3 \\ x_4 \end{bmatrix} + \begin{bmatrix} 0 & 0 \\ 1 & 0 \\ 0 & 0 \\ 0 & 1 \end{bmatrix} \begin{bmatrix} \ddot{X}_{pm} \\ \ddot{Y}_{pm} \end{bmatrix} + \begin{bmatrix} 0 & 0 \\ 1 & 0 \\ 0 & 0 \\ 0 & 1 \end{bmatrix} \begin{bmatrix} w_1 \\ w_2 \end{bmatrix} \tag{42}$$
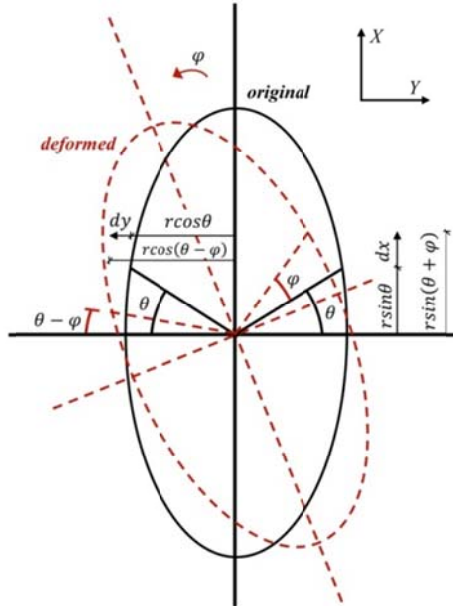

Fig. 16 Calculation of the angle of rotation of the inner tube oval section in the X-Y plane

where $\ddot{X}_{pm}$, $\ddot{Y}_{pm}$ are the measured accelerations, and w_1, w_2 are the associated process noise sources assumed to be white Gaussian noise processes. The observation equation is based on the GPS measurements X_{0m}, Y_{0m} obtained at a lower sampling rate. Using both of the equations in (31) this can be written as

$$
\begin{aligned}
\varphi_1 &= \theta - \cos^{-1}\left(\cos\theta - \frac{x_3 - Y_{0m}}{r}\right) \\
z_1 &= X_{0m} = x_1 - \Delta x = x_1 - r\sin(\theta + \varphi_1) + r\sin\theta + \upsilon_1 \\
\varphi_2 &= \sin^{-1}\left(\sin\theta + \frac{x_1 - X_{0m}}{r}\right) - \theta \\
z_2 &= Y_{0m} = x_3 - \Delta y = x_3 + r\cos(\theta - \varphi_2) - r\cos\theta + \upsilon_2
\end{aligned}
\tag{43}
$$

where the measured quantity z_1 is assumed to be equal to the GPS displacements, X_{0m}, in the x direction and involves the calculation of ϕ which in turn depends on the measured GPS displacement, Y_{0m}, in the y direction. The second component of the measurement vector $z = [X_{0m} \; Y_{0m}]^T$ is defined accordingly for the other direction. As mentioned earlier, ρ, θ, are known constants and $\upsilon = [\upsilon_1 \; \upsilon_2]^T$ is the measurement noise, assumed to be white Gaussian.

By employing numerical integration at a sampling interval of T_a, the system Eq. (42) and the observation Eq. (43) can be written in compact discrete form

$$
\begin{aligned}
\mathbf{x}_{k+1} &= \mathbf{A}_d\mathbf{x}_k + \mathbf{B}_d\mathbf{x}_{pm} + \mathbf{w}_k \\
\mathbf{y}_k &= H(\mathbf{x}_k) + \mathbf{v}_k
\end{aligned}
\tag{44}
$$

In the above equation, notice how the observation is in fact a nonlinear function, $\mathbf{H}$, of the state.

5.2 Implementation and results

In order to produce simulations of the above system, time histories for the $\ddot{X}_p$, $\ddot{Y}_p$, ϕ signals are initially generated and the GPS measurement signals X_0, Y_0 are subsequently reproduced using Eq. (43). We then proceeded to contaminate the original X_p, Y_p accelerometer measurements with a low level of random white noise (noise to signal RMS ratio $\approx 1\%$). The finally obtained time histories of the GPS and integrated accelerometer signals are plotted in Figs. 17 and 18 for a time segment of 5 min out of the total 40 min of produced records.

It should be noted here that for the derivation of the X_p, Y_p displacement signals, the noisy accelerometer readings $\ddot{X}_p$, $\ddot{Y}_p$ need to be properly filtered with a high-pass filter ($f_c = 0.02 Hz$) in order to avoid the drifting effect due to low frequency noise content. In addition, the signal is also detrended after numerical integration. This process, is quite invasive and may

ultimately lead to substantially different estimates for X_p, Y_p, as observed in Figure 18, which may more importantly yield inaccurate estimates for the section angle of rotation ϕ. Naturally, when using this noisy input for the two independent formulas of Eq. (40) for deriving ϕ, we are bound to obtain significantly divergent estimations for the angle of rotation. In Fig. 19 the estimates of ϕ are compared to the assumed clean estimate (which is unique) for three cases; a) for the noisy signals corresponding to Figs.17 and 18(b)) for $\ddot{X}_p$, $\ddot{Y}_p$, signals contaminated with a higher white noise level of 1.5% RMS ratio; and c) for signals generated using a high pass filter with a lower cutoff frequency ($f_c = 0.01$).
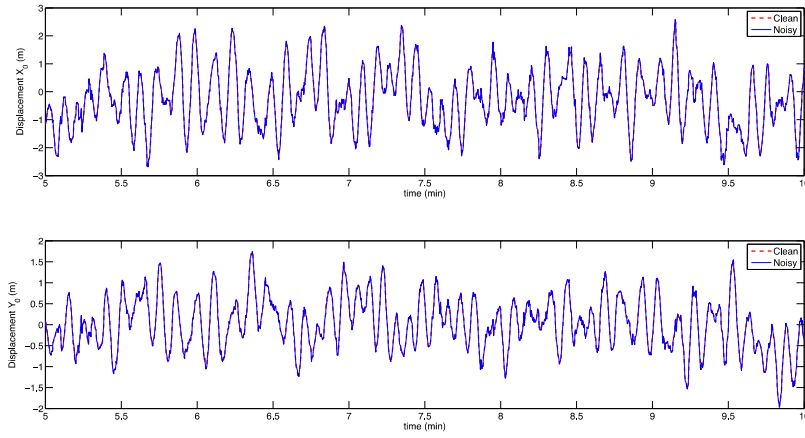

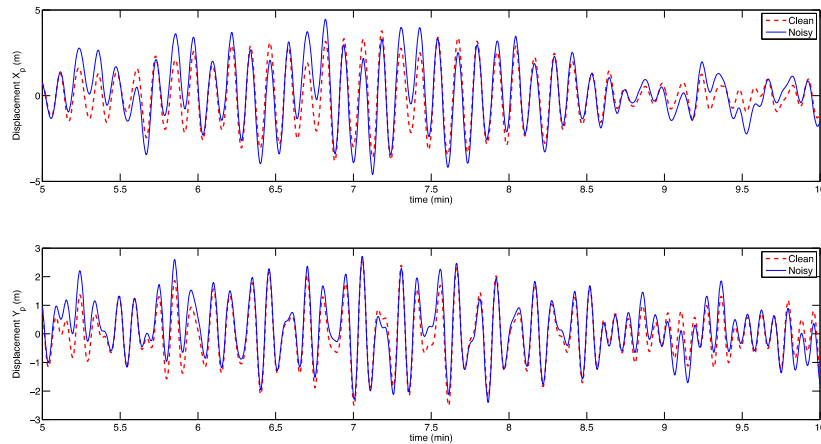Fig. 17 GPS in-plane displacement time histories

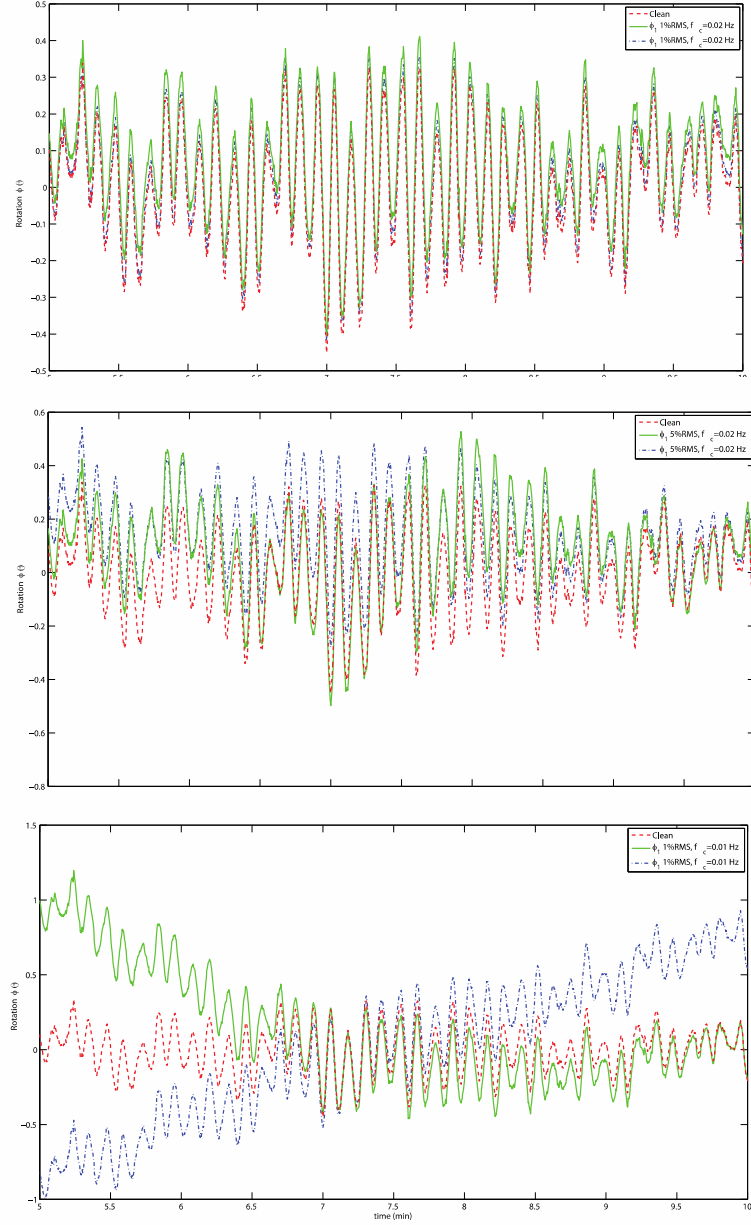Fig. 18 Accelerometer derived displacement time histories

Fig. 19 Time history for angle of rotation ϕ a) for the noisy $\ddot{X}_p$, $\ddot{Y}_p$, X_0, Y_0 signals corresponding to Figs. 17 and 18(b)) for $\ddot{X}_p$, $\ddot{Y}_p$ signals contaminated with a higher white noise level of 5%RMS ratio; and c) for signals generated using a high pass filter with a lower cutoff frequency ($f_c = 0.01 Hz$)

In Fig. 19, ϕ_1, ϕ_2, denote the angle of rotation estimates as these are obtained from the two independent formulas of Eq. (40). As is obvious in the figure, both the noise level as well as the post-processing of the acceleration signals, involving filtering and detrending, critically influence the finally obtained estimates of rotation ϕ. In previous works, for this purpose, averaging of the two deviant results obtained from each geometric relation was performed in order to yield the final estimate. Obviously this procedure, other than highly inefficient for significant noise levels, is also not suitable for online monitoring applications, as both filtering and detrending are based on the availability of a significant portion of data. In this work we explore whether the online identification method we propose can cope with these issues. Initially, the multi-rate UKF regime described in section 2.3 was implemented. In addition, the Unscented Rauch-Tung-Striebel (URTS) Smoother of section 2.4 was applied in an effort to circumvent the drift problem which is expected to occur during integration which takes place when moving from the continuous time setup to the discretized equivalent.

Fig. 21 demonstrates the finally estimated X_p, Y_p time series, making it clear that the smoother is not enough to circumvent the drift in the displacement estimates. Although, the filter is able to successfully track the observations X_0, Y_0 (Fig. 20) drifted estimates for the X_p, Y_p and ϕ time histories are produced which is clearly unsuitable for monitoring purposes. An alternative process is needed which can exempt us from this reliance on the integrated data and most importantly render the process online so that it is suitable for active control applications. The problem is more pronounced during the first steps of the analysis. The noise content of both the GPS and acceleration signals as well as the fact that the two are non-collocated constitute the drift correction a non trivial task.
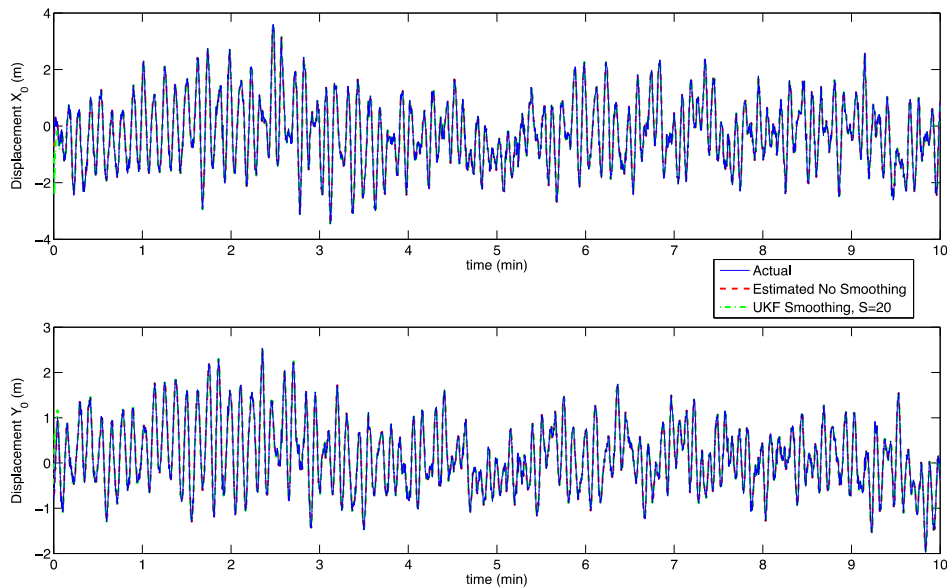

Fig. 20 Estimates of the observed quantities X_0, Y_0 with and without the UKF Smoother
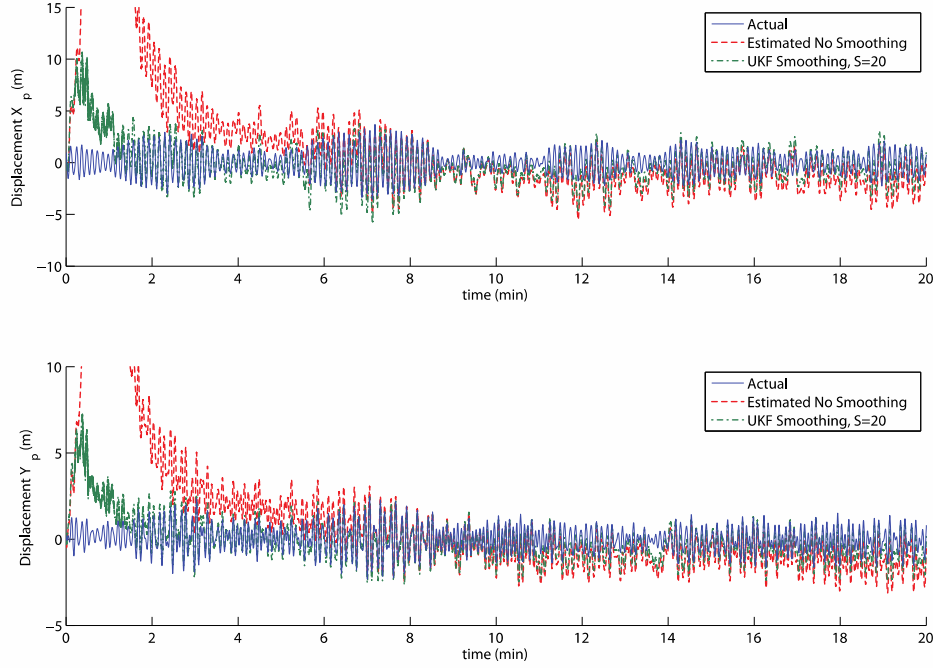
Fig. 21 Estimates of the unmeasured states X_p, Y_p with and without the UKF Smoother

We try to tackle the problem by implementing the artificial white noise observation scheme proposed herein. Two extra observations are assumed in place of the unobserved X_p, Y_p time histories, corresponding to zero mean white noise (WN) signals of low variance. For this purpose, Eq. (43) is now modified to include artificial WN observations for X_p, Y_p

$$
\begin{aligned}
y_1^k &= X_0 = x_1^k - r\sin(\theta + \varphi_1^k) + r\sin\theta + \upsilon_1^k \\
y_2^k &= Y_0 = x_3^k - r\cos(\theta - \varphi_2^k) + r\cos\theta + \upsilon_2^k \\
y_3^k &= X_p = x_1^k + \upsilon_3^k \\
y_4^k &= Y_p = x_3^k + \upsilon_4^k
\end{aligned}
\tag{36}
$$

Therefore no educated assumption is made upon them, nonetheless as it turns out from the estimation results this is enough to account for the drifting effect. The X_p, Y_p estimates are forced to not drift as the estimation evolves. For the results presented in Figs. 22 and 23, an observation noise level of $\sim 30\%$ RMS ratio to the actual displacement signal (X_p, Y_p) is assumed for υ_3, υ_4.
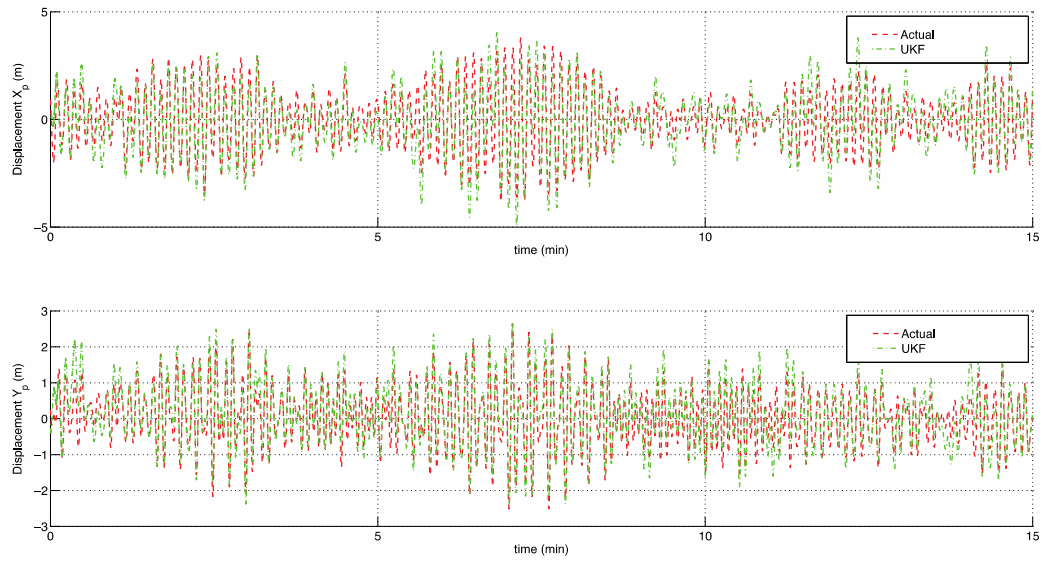
Fig. 22 Displacement time histories for accelerometer sensor points, using the artificial white noise observations
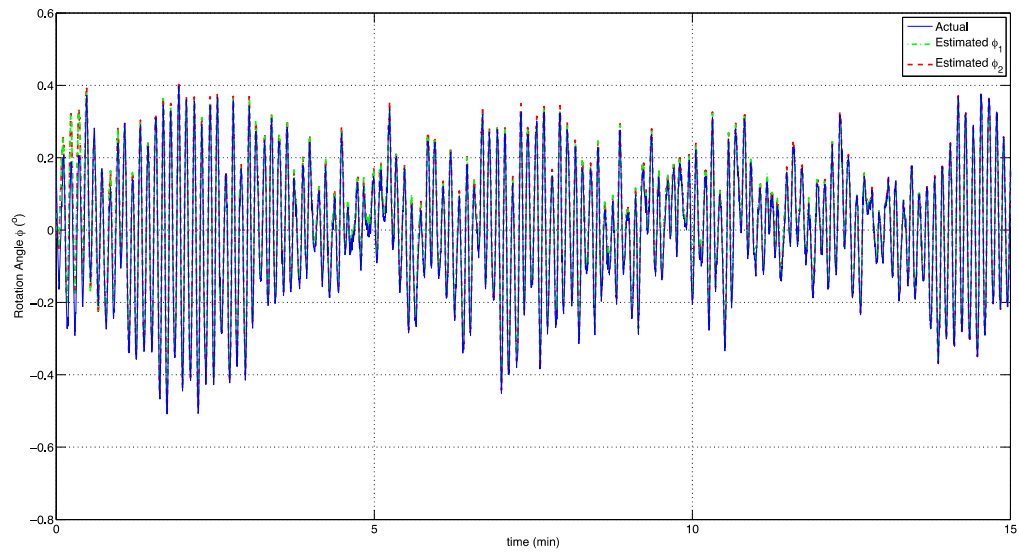

Fig. 23 Time history for angle of rotation (UKF estimate), using the artificial white noise observations

As shown schematically in Figs. 22 and 23 the UKF is now successful in tracking X_p, Y_p, while the two ϕ estimates are now very well weighted with an absolute error norm of merely 1.2%. An alternative process could be pursued, in an off-line scenario, by feeding the filtered, integrated and detrended (and therefore biased) X_p, Y_p results into the observer in the place of the artificial observations. As it turns out, the normalized root mean square deviation (NRMSD) of the ϕ_1, ϕ_2 estimates with respect to the actual ϕ time history, is somewhat improved when using the artificial observation approach versus the off-line scheme. The relevant numbers for the off-line scheme and the online artificial WN observation approach are

$$\text{off-line:} \quad \frac{\|\phi_1 - \phi\|}{\|\phi\|} = 0.044 \quad \& \quad \frac{\|\phi_2 - \phi\|}{\|\phi\|} = 0.043$$

$$\text{online:} \quad \frac{\|\phi_1 - \phi\|}{\|\phi\|} = 0.032 \quad \& \quad \frac{\|\phi_2 - \phi\|}{\|\phi\|} = 0.031$$

(46)

where the NRMSD is defined as:

$$NRMSD(\phi_i) = \sqrt{\frac{\sum_{i=1}^{N} (\phi_i - \phi)^2}{N(\phi_{max} - \phi_{min})}}$$

(47)

(a) NRMSD of the X_0, Y_0 estimates   (b) NRMSD of the ϕ_1, ϕ_2
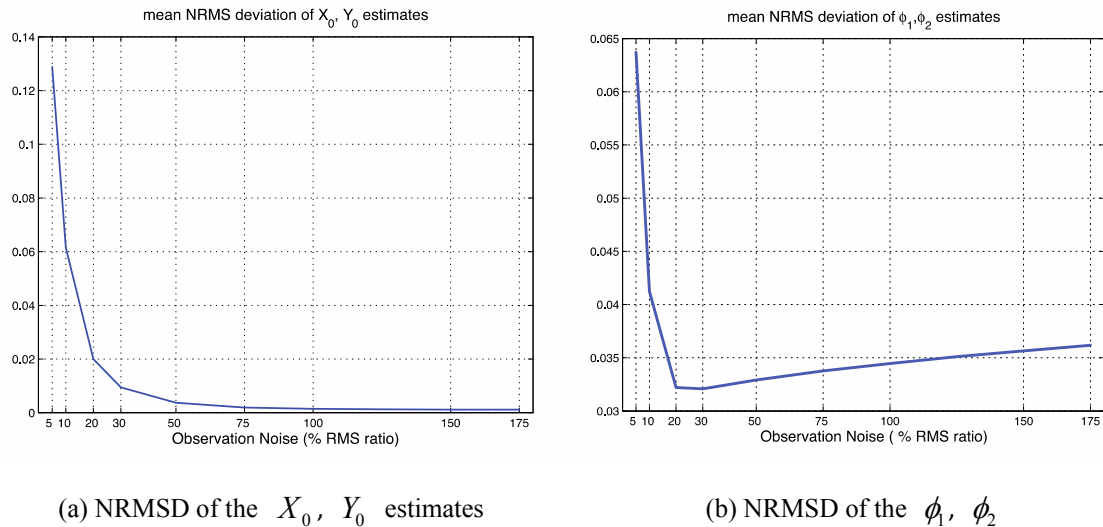
Fig. 24 Mean normalized root mean square deviation (NRMSD) of the X_0, Y_0, ϕ estimates

In order to explore how sensitive this technique is to the assumed artificial noise level, parametric runs were performed for different values of the added noise. Figs. 24 (a) and (b) display the relevant NRMSD plots for the ϕ and GPS displacement estimates (X_0, Y_0). These indicate that the estimate accuracy seems to be rather insensitive to the choice of observation noise level, as long as it is not a very low one (above 10% RMS yields good performance).

5. Conclusions

A numerical procedure for the online correction of integrated quantities, such as displacements and rotations, has been proposed in this study. The online tracking of such quantities, which is sought for monitoring and control purposes, is not a trivial task as noise contamination often leads in imprecise estimation due to integration errors. For this purpose:

• A new approach based on a time domain identification method, namely the Unscented Kalman Filter (UKF), is proposed for correcting the "drift effect" in the displacement or rotation estimates on-the-fly as data is attained.

• The method relies on the introduction of artificial white noise (WN) observations into the filter equations in place of the unobserved integral quantities. This scheme renders the estimation process real-time while, at the same time, proves relatively insensitive to the selection of observation noise level.

• The efficacy of the proposed approach is demonstrated for the simple example of a sdof linear oscillator where availability of acceleration measurements is exclusively assumed.

• In a second application, a data fusion problem for the torsional identification of a tall tower structure is investigated. A multi-rate Kalman Filter is incorporated into the analysis in order to successfully fuse data sampled at different rates. The proposed scheme is shown to outperform alternative, "near online" correction methodologies such as smoothing.

• The approach introduced herein, alleviates the need for filtering and detrending before proceeding to integration of accelerometer data, which would lead to an off-line process. Moreover, the applications demonstrate the robustness of the method, even in presence of significant levels of noise, provided an underlying physical, geometric or analytical model of the system is available.

References

Basseville, M., Benveniste, A., Goursat, M. and Mevel, L. (2007), "In-flight vibration monitoring of aeronautical structures", *IEEE Control Syst. Mag.*, **27**(5), 27-42.

Beck, J., Au, S. and Vanik, M. (1999), "A bayesian probabilistic approach to structural health monitoring", *American Control Conference Proceedings*, **2**, 1119-1123.

Berg, G. and Housner, G.W. (1961), "Integrated velocity and displacement of strong earthquake ground motion", *B. Seismol. Soc. Am.*, **51**(2), 175-189.

Boore, D.M. and Bommer, J.J. (2005), "Processing of strong-motion accelerograms: needs, options and consequences", *Soil Dyn. Earthq. Eng.*, **25**(2), 93-115.

Bucharles, A. and Vacher, P. (2002), "Flexible aircraft model identification for control law design", *Aerosp. Sci. Technol.*, **6**(8), 591-598.

Casciati, F., Saleh, R.A. and Fuggini, C. (2009), "GPS-based SHM of a tall building: torsional effects",

Proceedings of the 7th International Workshop on Structural Health Monitoring, 9-11 September 2009, Stanford University, Stanford.

Chatzi, E.N. and Smyth, A.W. (2009), "The unscented kalman filter and particle filter methods for nonlinear structural system identification with non-collocated heterogeneous sensing", *Struct. Control Health Monit.*, **16**(1), 99-123.

Chatzi, E.N., Smyth, A.W. and Masri, S.F. (2010), "Experimental application of on-line parametric identification for nonlinear hysteretic systems with model uncertainty", *Struct. Saf.*, **32**(5), 326 -337.

Chen, T., Morris, J. and Martin, E. (2005), "Particle Filters for state and parameter estimation in batch processes", *J. Process Contr.*, **15**(6), 665-673.

Doebling, S.W., Farrar, C.R., Prime, M. and Shevitz, D.W. (2009), *Damage identification and health monitoring of structural and mechanical systems from changes in their vibration characteristics: A literature review*, Technical Report, Los Alamos National Lab, NM (United States).

Faravelli, L., Casciati, S. and Fuggini, C. (2009), "Full-scale experiment using GPS sensors for dynamic tests", *Proceedings of the XIX Congress AIMETA*, September 14-17, 2009, Ancona.

Faravelli, L., Ubertini, F. and Fuggini, C. (2010), "Subspace Identification of the Guangzhou new TV Tower", *Proceedings of the 5th World Conference on Structural Control and Monitoring*, July 12-14, 2010, Shinjuku, Tokyo.

Faravelli, L., Ubertini, F. and Fuggini, C. (2010), "System identification toward FEM updating of a super high-rise buildings", *Proceedings of the 5th European Workshop on Structural Health Monitoring*, June 28 July 2, 2010, Sorrento, Italy.

Faravelli, L., Ubertini, F. and Fuggini, C. (2011), "System identification of a super high-rise building via a stochastic subspace approach", *Smart Struct. Syst.*, **7** (2), 133-152.

Fraraccio, G.A., Brügger, A. and Betti, R. (2008), "Identification and damage detection in structures subjected to base excitation", *Experimental Mech.*, **48**(4), 521-528.

Fuggini, C. (2009), *Using Satellites Systems for Structural Monitoring: Accuracy, Uncertainty and Reliability*, PhD Dissertation, University of Pavia, Pavia, Italy.

Gao, Y., Spencer, B.F. and Ruiz-Sandoval, M. (2006), "Distributed computing strategy for structural health monitoring", *Struct. Control Health Monit.*, **13**(1), 488-507.

Hong, A., Ubertini, F. and Betti, R. (2013), "New stochastic subspace approach for system identification and its application to long-span bridges", *J. Eng. Mech. – ASCE*, **139**(6), 724-736.

Julier, S.J. and Uhlmann, J.K. (1997), "A new extension of the Kalman Filter to nonlinear systems", *Proceedings of AeroSense: The 11th Int. Symposium on Aerospace/Defense Sensing, Simulation and Controls*, Orlando.

Kim, J., Kim, K. and Sohn, H. (2014), "Autonomous dynamic displacement estimation from data fusion of acceleration and intermittent displacement measurements", *Mech. Syst. Signal Pr.*, **42**(12), 194-205.

Lin, J.W., Betti, R., Smyth, A.W. and Longman, R.W. (2001), "On-line identification of non-linear hysteretic structural systems using a variable trace approach", *Earthq. Eng. Struct. D.*, **30**(9), 1279-303.

Lourens, E., Papadimitriou, C., Gillijns, S., Reynders, E., De Roeck, G. and Lombaert, G. (2012), "Joint input-response estimation for structural systems based on reduced-order models and vibration data from a limited number of sensors", *Mech. Syst. Signal Pr.*, **29**, 310-327.

Mani, G., Quinn, D.D. and Kasarda, M.E.F. (2006), "Structural Health Monitoring of Rotordynamic Systems by Wavelet Analysis", *ASME Conference Proceedings 2006* (4773X), 685-692.

Mariani, S. and Corigliano, A. (2005), "Impact induced composite delamination: state and parameter identification via joint and dual extended kalman filters", *Comput. Method. Appl. M.*, **194**(50-52), 5242-5272.

Maskell, S. and Gordon, N.A. (2001), "Tutorial on particle filters for on-line nonlinear/non-gaussian bayesian tracking", *IEEE T. Signal Proces.*, **50**(2), 174-188.

Moschas, F. and Stiros, S. (2012), "Phase effect in time-stamped accelerometer measurements: an experimental approach", *Int. J. Metrol. Quality Eng.*, **3**, 161-167.

Moaveni, B., He, X., Conte, J.P. and Restrepo, J.I. (2010), "Damage identification study of a seven-story full-scale building slice tested on the UCSD-NEES shake table", *Struct. Saf.*, **32**(5), 347-356

Naets, F., Pastorino, R., Cuadrado, J. and Desmet, W. (2013), "Online state and input force estimation for multibody models employing extended kalman filtering", *Multibody Syst. Dyn.*, 1-20

Papadimitriou, C., Fritzen, C., Kraemer, P. and Ntotsios, E. (2011), "Fatigue predictions in entire body of metallic structures from a limited number of vibration sensors using kalman filtering", *Struct. Control Health Monit.*, **18**(5), 554-573.

Park, J.W., Sim, S.H. and Jung, H.J. (2013), "Displacement estimation using multimetric data fusion", *IEEE/ASME T. Mechatronics*, **18**(6), 1675-1682.

Psimoulis, P.A. and Stiros, S.C. (2008), "Experimental assessment of the accuracy of GPS and RTS for the determination of the parameters of oscillation of major structures", *Comput.-Aided Civil Infrastruct. E.*, **23**(5), 389-403.

Rajamani, M.R. (2007), *Data-based Techniques to Improve State Estimation in Model Predictive Control*, PhD Thesis, University of Wisconsin-Madison, October 2007

Rajamani, M.R. and Rawlings, J.B. (2009), "Estimation of the disturbance structure from data using semidefinite programming and optimal weighting", *Automatica*, **45**,142-148.

Rauch, H.E., Striebel, C.T. and Tung, F. (1965), "Maximum likelihood estimates of linear dynamic systems", *J. Am. Inst. Aeronaut. Astronaut.*, **3**(8), 1445-50.

Ristic, B., Arulampalam, S. and Gordon, N. (2004), "Beyond the Kalman filter: Particle filters for tracking applications", Artech house.

Sarkka, S. (2008), "Unscented Rauch-Tung-Striebel smoother", *IEEE T.Automat. Control.*, **53**(3), 845-549.

Smyth, A. and Wu, M. (2007), "Multi-rate kalman filtering for the data fusion of displacement and acceleration response measurements in dynamic system monitoring", *Mech. Syst. Signal Pr.*, **21**(2), 706-723.

Stiros, S., Psimoulis, P. and Kokkinou, E. (2008), "Errors introduced by fluctuations in the sampling rate of automatically recording instruments: Experimental and theoretical approach", *J. Surv. Eng. - ASCE,* **134**(3), 89-93.

Stiros, S.C. (2008), "Errors in velocities and displacements deduced from accelerographs: An approach based on the theory of error propagation", *Soil Dynam. Earthq. Eng.*, **28**(5), 415-420.

Terejanu, G., Singh, T. and Scott, P. (2007), "Unscented kalman filter/smoother for a CBRN puff-based dispersion model", *Proceedings of the 10th International Conference on Information Fusion*, 9-12 July.

Wan, E. and Van Der Merwe, R. (2000), "The unscented kalman filter for nonlinear estimation", *Adaptive Systems for Signal Processing, Communications, and Control Symposium*, AS-SPCC, IEEE, Lake Louise, Alberta, Canada. Oct 2000, **153**-8.

Yuen, K.V. and Katafygiotis, L.S. (2006), "Substructure identification and health monitoring using noisy response measurements only", *Comput. - Aided Civil Infrastruct. E.*, **21**(4), 280-291.